JOURNAL OF GEOPHYSICAL RESEARCH, VOL. 112, D06309, doi:10.1029/2005JD006556, 2007

Effects of additional nonmethane volatile organic compounds, organic nitrates, and direct emissions of oxygenated organic species on global tropospheric chemistry

Akinori Ito,[1,2] Sanford Sillman,[1] and Joyce E. Penner[1]

Received 3 August 2005; revised 21 July 2006; accepted 17 August 2006; published 29 March 2007.

[1] This work evaluates the sensitivity of tropospheric ozone and its precursors to the representation of nonmethane volatile organic compounds (NMVOCs) and organic nitrates. A global 3-D tropospheric chemistry/transport model (IMPACT) has been exercised initially using the GEOS-Chem chemical reaction mechanism. The model was then extended by adding emissions and photochemical reactions for aromatic and terpenoid hydrocarbons, and by adding explicit representation of hydroxy alkyl nitrates produced from isoprene. Emissions of methanol, phenol, acetic acid and formic acid associated with biomass burning were also added. Results show that O_3 increases by 20% in most of the troposphere, peroxyacetyl nitrate (PAN) increases by 30% over much of the troposphere and OH increases by 10%. NO_x ($NO + NO_2$) decreases near source regions and increases in remote locations, reflecting increased transport of NO_x away from source regions by organic nitrates. The increase in O_3 was driven largely by the increased role of PAN as a transporter of NO_x and by the rerelease of NO_x from isoprene nitrates. The increased PAN production was associated with increases in methyl glyoxal and hydroxyacetone. Comparison with measured values show reasonable agreement for O_3 and PAN, but model measurement agreement does not either improve or degrade in the extended model. The extended model shows improved agreement with measurements for methanol, acetic acid and peroxypropional nitrate (PPN). Results from the extended model were consistent with measured alkyl nitrates and glycolaldehyde, but hydroxyacetone and methyl glyoxal were overestimated. The latter suggests that the effect of the isoprene nitrates is somewhat smaller than estimated here. Although the model measurement comparison does not show specific improvements with the extended model, it provides a more complete description of tropospheric chemistry that we believe is important to include.

Citation: Ito, A., S. Sillman, and J. E. Penner (2007), Effects of additional nonmethane volatile organic compounds, organic nitrates, and direct emissions of oxygenated organic species on global tropospheric chemistry, *J. Geophys. Res.*, *112*, D06309, doi:10.1029/2005JD006556.

1. Introduction

[2] It is widely known that volatile organic compounds have a large influence on the photochemistry of the remote troposphere. Volatile organics are known to directly affect the chemistry of O_3, nitrates and OH and are also linked to the chemistry of CO and CH_4 [e.g., *Houweling et al.*, 1998; *Prather et al.*, 2003]. It has been shown that isoprene alone is responsible for a large fraction of the overall effects of all NMVOCs, especially in the tropics [*Wang et al.*, 1998b]. The effect of the nonmethane volatile organic compounds (NMVOCs) on the formation of ozone has been investigated using three dimensional chemistry transport models (CTM) [e.g., *Houweling et al.*, 1998; *Bey et al.*, 2001; *Prather et al.*, 2003].

[3] Because the chemistry of organics is complex, model assessments must use simplified representations of both NMVOC species and reaction pathways. Typically, these simplified mechanisms will represent many different VOC species as a single representative species or through a composite species with reactions that represent the combined pathways of several species. In many cases, certain species are omitted entirely for simplicity. Many studies of tropospheric chemistry have routinely omitted aromatic species [e.g., *Bey et al.*, 2001] even though these may represent as much as 30% of all emitted anthropogenic organics by carbon number. Biogenic terpenes are also often omitted from analyses of tropospheric photochemistry. Aromatic chemistry is neglected in part because of the computational cost and in part because of the expectation that the effect of aromatics on large-scale ozone budgets is

[1]Department of Atmospheric, Oceanic and Space Sciences, University of Michigan, Ann Arbor, Michigan, USA.
[2]Now at Frontier Research Center for Global Change, JAMSTEC, Yokohama, Japan.

0148-0227/07/2005JD006556$09.00

relatively small [*Houweling et al.*, 1998; *Horowitz et al.*, 1998]. Nevertheless, they may still affect chemistry at northern locations during winter, when emission rates for biogenic VOCs are low.

[4] In recent years considerable attention has been given to the secondary reaction products of isoprene, especially the isoprene nitrates. Although isoprene is the dominant volatile organic in terms of emissions, its direct impact on photochemistry is limited by its short atmospheric lifetime. The direct reaction products of isoprene, including methylvinyl ketone, methacrolein and formaldehyde, also have atmospheric lifetimes of a few hours. The chemistry of the subsequent reaction products of isoprene, especially isoprene nitrates and peroxides, is less well known, and the ultimate reaction products of isoprene include some species (e.g., hydroxyacetone) with longer atmospheric lifetimes.

[5] *Horowitz et al.* [1998] included the formation of isoprene nitrates in a global three-dimensional (3-D) model and their subsequent degradation into NO_x and volatile organics. They reported the large impact of isoprene on ozone formation in the troposphere, largely through its effect on the export of NO_x from source regions to the remote troposphere. Several earlier studies addressed the effect of organics as transporters of NO_x in box models and in global 3-D models [e.g., *Atherton and Penner*, 1988; *Penner et al.*, 1991; *Kasibhatla et al.*, 1993; *Emmons et al.*, 1997] and in general [*Singh and Hanst*, 1981; *Singh*, 1987]. *Bey et al.* [2001] showed 3-D model results that agreed with measured NO and PAN (from the compilation of *Emmons et al.* [2000]) to within a factor of two, despite the omission of aromatics and the assumption that isoprene nitrates undergo an aerosol reaction and are rapidly converted to HNO_3 and subsequently removed by dry deposition. *Pöschl et al.* [2000] reported that assumptions about isoprene nitrates can have a significant impact on photochemistry, on the basis of zero-dimensional calculations. More recently, *von Kuhlmann et al.* [2004] and *Fiore et al.* [2005] tested the impact of isoprene nitrate chemistry in global chemical transport models.

[6] Here, we present results from a model for global tropospheric chemistry with extensions for a number of commonly omitted species. The results are from the Integrated Massively Parallel Atmospheric Chemical Transport (IMPACT) model that was developed at the Lawrence Livermore National Laboratory (LLNL) [*Rotman et al.*, 2004] and at the University of Michigan [*Liu and Penner*, 2002; *Liu et al.*, 2005]. The model is exercised initially using a recent version of the photochemical mechanism associated with the GEOS-Chem model (M. J. Evans et al., 2003, The GEOS-CHEM Chemical Mechanism, Version 5-07-8, Harvard University, Cambridge, Massachusetts (available at http://www.env.leeds.ac.uk/~mat/GEOS-CHEM/geoschem_mech.pdf); hereinafter referred to as Evans et al., 2003), which has been widely used in previous global modeling studies [e.g., *Bey et al.*, 2001]. The analysis is then repeated using an extended version of the model with the following additions: (1) Emissions and photochemistry of aromatic hydrocarbons, including benzene, toluene and xylene as surrogates for all directly emitted aromatics. (2) Emissions and photochemistry of alpha-pinene and limonene as representatives of biogenic terpenes. (3) Representation of a hydroxyalkyl nitrate produced by the reaction of NO with RO_2 radicals derived from isoprene, methylvinylketone and methacrolein. (4) Direct emission of methanol, phenol, acetic acid, formic acid and acetone from biomass burning [*Ito and Penner*, 2004].

[7] The IMPACT model and updated photochemistry is described in section 2. Section 3 shows how model results are changed as a result of the extensions. Section 4 shows a comparison between model results and ambient measurements from the data set compiled by *Emmons et al.* [2000], which has been widely used for evaluating global 3-D models. We also show comparisons with individual field measurements for alkyl nitrates, methyl glyoxal and hydroxyacetone, which have added significance in the model with extended chemistry.

2. Methods

2.1. Global 3-D Model

[8] We investigate the effect of anthropogenic and biogenic NMVOCs on tropospheric ozone and its precursors using the IMPACT model [*Rotman et al.*, 2004], with a modified numerical solution for photochemistry [*Sillman*, 1991] and a modified chemical mechanism. In these simulations, we used meteorological fields for 1997 from the National Aeronautics and Space Administration (NASA) Data Assimilation Office (DAO) GEOS-STRAT (Goddard EOS Assimilation System-Stratospheric Tracers of Atmospheric Transport) model [*Coy and Swinbank*, 1997; *Coy et al.*, 1997]. The meteorology was defined on a 4° latitude × 5° longitude horizontal grid with 46 vertical layers. The model was exercised for a 1-year time period with a 4-month spin-up time, and with emissions (described below) based on 1997. This model has been exercised previously under the NASA Global Modeling Initiative (GMI) [*Rodriguez et al.*, 2004] using the photochemical mechanism from the GEOS-Chem model, version 5-07-8 (Evans et al., 2003). As described below, the same chemistry is used in one of the two cases described here.

[9] Photolysis rate constants are calculated using the Fast-J radiative transfer model [*Wild et al.*, 2000] with $O(^1D)$ quantum yields updated to JPL2003 [*Sander et al.*, 2003]. Cloud optical depths are determined using the random overlap treatment described by *Feng et al.* [2004], which assumes that cloudy and cloud-free subregions in each model grid box randomly overlap with cloudy and cloud-free subregions in grid boxes located above or below [*Briegleb*, 1992]. This replaces the simpler method used by *Rodriguez et al.* [2004], which represents cloud properties in each grid box as a linear average of cloudy and cloud-free subregions and calculates optical depths based on a vertical path through grid-wide average clouds. In addition, monthly average concentrations of SO_2, sulfate aerosol and dimethyl sulfide (DMS) were taken from a separate run of the IMPACT model for aerosols [*Liu et al.*, 2005]. These concentrations were used in the current model run to calculate the effect of aerosols on photolysis rates. They were also used to calculate the rates of reaction of gas-phase species on aerosol surfaces and rates of reaction involving SO_2 and DMS, as part of the calculation of photochemical production and loss.

[10] Transport is calculated individually for most species, but in a few cases closely related species are transported as a

Table 1. Solubility Parameters Used in the Dry and Wet Deposition Parameterizations

Species	H298[a], moles L^{-1} atm^{-1}	$-\Delta H/R$[a], °K	References
Hydroxyalkyl peroxides and others from biogenic sources	1,700,000	9,700	*O'Sullivan et al.* [1996]
HNO_3	210,000	8,700	*Schwartz and White* [1981]
glyoxal(CHOCHO)	360,000		*Zhou and Mopper* [1990]
H_2O_2	83,000	7,400	*O'Sullivan et al.* [1996]
hydroxyethanal($HOCH_2CHO$)	41,000	4,600	*Betterton and Hoffmann* [1988]
Alkyl nitrates and hydroxyalkyl nitrates from biogenics	17,000	9,200	*Treves et al.* [2000]; *Shepson et al.* [1996]
HNO_4	12,000	6,900	*Régimbal and Mozurkewich* [1997]
Formic acid (HCOOH)	8,900	6,100	*Johnson et al.* [1996]
Acetic acid (CH_3COOH)[b]	4,100	6,300	*Johnson et al.* [1996]
Methyl glyoxal(CH_3COCHO)	3,700	7,500	*Betterton and Hoffmann* [1988]
Hydroxyacetone	2927	0	*Spaulding et al.* [2002]
HCHO	3,200	6,800	*Staudinger and Roberts* [1996]
Organic peroxides with the form ROOH (based on $C_2H_5O_2H$)	340	6,000	*O'Sullivan et al.* [1996]
CH_3CO_2H	312	5,200	*O'Sullivan et al.* [1996]

[a]The effective Henry's law constant is used for acids (HNO_3, HCOOH, CH_3COOH, and CH_3CO_3H). $H_{eff} = H_{298} \times (1 + K_a/[H+])$, $[H+] = 10^{-5}$, K_a = 15.1 (HNO_3 [*Schwartz and White*, 1981]), $K_a = 1.78e^{-4}$ (HCOOH [*Lide*, 1999]), $1.74e^{-5}$ (CH_3COOH and CH_3CO_3H [*Lide*, 1999]). The adjustment for temperature is as follows: $H_T = H_{298} \times \exp[(-delH/R) \times (1/T-1/298)]$.

[b]Wet deposition for acetic acid was included only in the simulation with extended chemistry.

group sum. These summed species include the following: $\geq$C3 RO_2 radicals; nitrate-containing RO_2's; RCO_3 radicals; radicals produced from reactions of biogenics with NO_3; $\geq$C3 organic peroxides from anthropogenic sources; organic peroxides from isoprene reaction products; organic peroxides from terpenes; alkyl nitrates produced from alkanes; and higher PANs produced from aromatics. The sums all involve species that are photochemically similar. The transported sums were also chosen to insure that primarily anthropogenic species and primarily biogenic species are kept distinct from one another. The photochemical calculation partitions each transported sum into individual components on the basis of the rate of photochemical production of each individual species. This treatment was found to have negligible difference on results in zero-dimensional (0-D) calculations.

[11] In order to account for O_3 chemistry in the stratosphere, the additional tracer, synthetic ozone (Synoz), is implemented to yield a stratospheric source of 475 Tg O_3 yr^{-1} [*McLinden et al.*, 2000]. The treatment of stratospheric HNO_3 is similar to that described by *Penner et al.* [1998]. The 150-ppbv isopleth of the monthly averaged distribution of the synthetic O_3 tracer is used to define the tropopause. Above this isopleth, the effects of stratospheric chemistry are simulated by imposing OH destruction on many species to ensure that they are not returned to the troposphere, while tropospheric chemistry is applied below this isopleth [*Wild and Prather*, 2000].

[12] The original (base) version of the model has acetone set to prescribed values derived from *Jacob et al.* [2002]. This is replaced by a complete simulation of acetone (including emissions, chemistry, transport and deposition) in the extended version.

[13] As described by *Rotman et al.* [2004], IMPACT calculates dry deposition loss rates using the dry deposition algorithm of *Wang et al.* [1998a], which follows the methodology of *Wesely et al.* [1985]. This method is used for the following species: NO_2, O_3, PAN, HCHO, H_2O_2, methyl peroxide, HNO_3, peroxymethacryloyl nitrate ($CH_3 = CCH_3CO_3NO_2$, or MPAN), peroxypropional nitrate (PPN), and summed, $\geq$C4 alkyl nitrates. The Harvard wet scavenging model [*Mari et al.*, 2000; *Liu et al.*, 2001] which is enhanced from previous models [*Giorgi and Chameides*, 1986; *Balkanski et al.*, 1993] is used for HNO_3, HCHO, H_2O_2, and methyl peroxide. Species scavenging depends on solubility through the Henry's law coefficient. The extended chemistry (described in section 2.2 below) includes several additional species that are removed by wet and dry deposition. Table 1 shows Henry's law coefficients for these species, which are largely based on the compilations by R. Sander, Compilation of Henry's Law Constants for inorganic and organic species of potential importance in environmental chemistry (Version 3), 1999 (available at http://www.mpch-mainz.mpg.de/~sander/res/henry.html) and *von Kuhlmann et al.* [2003a]. In addition, the simulation with extended chemistry includes wet deposition for acetic acid (based on Henry's law coefficients in Table 1) that had been omitted in the base chemistry simulation. The additional dry deposited species in the simulation with extended chemistry include all additional PAN-like organic nitrates, alkyl- and hydroxyalkyl nitrates (at the same rate as HNO_3), and acetone.

2.2. Photochemical Mechanisms

[14] The model has been exercised using two photochemical mechanisms. The first mechanism is identical to the mechanism used by the GEOS-Chem model, version 5-07-8 (Evans et al., 2003) (referred to below as the base mechanism). The second mechanism (referred to below as the extended mechanism) includes all the reactions of the base mechanism, along with extensions and modifications described here.

[15] The extended chemistry includes explicit representation of the following species, which are not included in the base mechanism from Evans et al.: three representative aromatic species (benzene, toluene and m-xylene); ethene;

Table 2. Emissions of Nonmethane Volatile Organic Compounds[a]

	Original	Extended
Anthropogenic Emissions		
Methylethyl ketone	5.8	5.8
C_2H_6	9.3	9.3
C_3H_8	7.3	7.3
CH_3CHO	3.3	3.3
HCHO	2.4	2.4
C4–C5 alkanes (ALK4)	26.6	15.3
≥C6 alkanes (ALK7)	0.0	11.3
Ethene	0.0	17.8
Propene	18.1	11.3
Trans-2-butene	0.0	6.6
Benzene	0.0	3.2
Toluene	0.0	5.8
m-xylene	0.0	5.5
Acetone	Fixed concentrations	3.5
Methanol	0	9.5
Formic acid	0	2.6
Acetic acid	0	12.4
Phenol	0	4.3
Total	72.6	132
Biogenic Emissions		
	Original	Extended
Isoprene	380	380
Propene	11	11
Ethene	0	9
Terpenes	CO[b]	82
Acetone	Fixed concentrations	20 (vegetation) + 17 (ocean)
Methanol	CO[c]	28

[a]In Tg C yr^{-1}, for the original simulation and the extended simulation.
[b]Biogenic source of CO from monoterpene oxidation.
[c]Biogenic source of CO from methanol oxidation.

trans-2-butene as a surrogate for internally bonded alkenes; species representing C4–C5 alkanes and ≥C6 alkanes (represented by a single species in original mechanism); two representative terpenes (alpha-pinene and limonene); and extended representation of hydroxyalkyl-nitrates produced from isoprene. The added partitioning of alkanes effectively increases the reactivity of these species by 33%. The extended mechanism also includes representation of various reaction products of the additional species. The extended mechanism includes a total of 178 species, of which 73 are transported, and 550 individual reactions. The base mechanism includes 105 species, of which 55 are transported, and 300 reactions. The simulation with extended chemistry requires approximately 30% more computation time. A complete listing of the additional and modified chemical reactions used in the extended chemistry is available at http://www-personal.umich.edu/~sillman/web-publications/Ito_2007_TableA1.pdf.

[16] The extended chemistry uses the isoprene mechanism proposed by *Paulson and Seinfeld* [1992] with modifications based on updated isoprene-related reaction rate coefficients, products, and reaction yields [*Carter*, 2000; *Atkinson and Arey*, 2003; *Atkinson et al.*, 2004; *Treves and Rudich*, 2003; R. Atkinson et al., Summary of Evaluated Kinetics and Photochemical Data for Atmospheric Chemistry, 2003, available at http://www.iupac-kinetic.ch.cam.ac.uk/summary/IUPACsumm_web_latest.pdf; hereinafter referred to as Atkinson et al., 2003].

[17] Most of the reactions involving isoprene and its reaction products are identical to the mechanism of Evans et al. (2003). However, our representation is different in that it includes explicit formation of hydroxyalkyl nitrates from the reaction of NO with RO_2 radicals produced by isoprene. In the mechanism of Evans et al. and in previous studies by *Bey et al.* [2001] it is assumed that most hydroxyalkyl nitrates are rapidly converted to HNO_3 and represents them as a direct production of HNO_3. This assumption can affect tropospheric chemistry in regions at some distance from NMVOCs and NO_x sources, because loss rates of hydroxyalkyl nitrates depend on the abundance of OH and deposition rates [*Treves and Rudich*, 2003; *von Kuhlmann et al.*, 2004]. We also assume that the radical produced by the reaction of isoprene with NO_3 subsequently reacts to produce an organic nitrate rather than HNO_3. Analogous changes are made for methylvinyl ketone, methacrolein and other isoprene reaction products. Subsequent reactions of organic nitrates produced from isoprene and its reaction products are taken from *Paulson and Seinfeld* [1992]. These changes ensure that the formation of hydroxyalkyl nitrates from isoprene does not represent a sink of organic carbon, unless removal through wet and dry deposition is calculated explicitly.

[18] Aromatics are represented as three explicit species: benzene, toluene (as a surrogate for all alkylbenzenes) and m—xylene (as a surrogate for dialkyl- and trialkylbenzenes). This representation is based on the work of *Lurmann et al.* [1986] as modified by *Jacob et al.* [1989] with updated reaction rates from *Atkinson and Arey* [2003]. We have used this rather than more recent mechanisms [*Carter*, 2000] because the latter mechanism uses operator species which assume that RO_2 radicals react instantly with NO. This assumption is invalid for the remote troposphere. Representation of ethene and *trans*-2-butene are also from *Lurmann et al.* [1986] with updated rate constants from *Atkinson et al.* [2004] and Atkinson et al. (2003). Representation of alpha-pinene and limonene is based on the work of *Stockwell et al.* [1997] with updates for the reaction of nitrate species from *Treves and Rudich* [2003].

[19] Some reactions involving organic peroxides have been modified in order to avoid confusion between anthropogenic and biogenic species. In the work of Evans et al. (2003) and in many other mechanisms, organic peroxides from biogenic sources react with OH to produce propionaldehyde, which acts as a surrogate for other aldehydes. We have replaced this with product species such as glycolaldehyde that have been identified as products of closely related species. For example, in the work of Evans et al. (2003) the peroxide VRP is formed from the RO_2 product of methylvinylketone and subsequently reacts with OH to form propionaldehyde. We have removed propionadelyde as a product in this reaction and added formaldehyde, glycolaldehyde and methyl glyoxal as reaction products, with stoichiometries in proportion to the product yield from the reaction of the RO_2 product of methyvinylketone with NO. This insures that the reaction sequences associated with isoprene only lead to products that are known to be formed from isoprene chemistry. We have also added removal reactions for >C2 organic acids, with rates and products analogous to those for acetic acid. In the original chemistry >C2 organic acids are nonreactive.

Table 3. Emissions of Nonmethane Volatile Organic Compounds[a]

	Open Vegetation Burning		Biofuel Burning	
Species	*Ito and Penner* [2004]	This work	*Ito and Penner* [2004]	This work
Phenol	0.0	0.2	4.1	4.1
Formic acid	1.0	2.2	0.3	0.3
Acetic acid	2.8	6.7	5.7	5.7
Methanol	1.9	5.1	3.3	3.3
Acetone	1.5	0.9	8.8	1.9

[a]In Tg C yr^{-1}, from biomass burning in this work compared to values from *Ito and Penner* [2004].

2.3. Emissions

[20] We use the emission inventory of NMVOCs described by *Bey et al.* [2001] for both the original and extended photochemical mechanisms. Table 2 summarizes the comparison of the emissions between the base and extended chemistry.

[21] The changes introduced here include (1) partitioning of emissions to reflect the more detailed speciation of alkanes and alkenes; (2) addition of anthropogenic emission of aromatics; (c) modification of biogenic emissions for terpenes and ethene; (3) addition of emissions of phenol, formic and acetic acid from biomass burning; and (4) addition of emission of methanol and acetone from all sources. The added emissions for aromatics, methanol, acetic acid, formic acid and phenol result in an emission rate for volatile organics in the extended simulation that is 177% of the equivalent emission rate in the original simulation in terms of total carbon. This ratio does not include acetone (which is set to a prescribed value in the original simulation) or biogenics. The added biogenic emission of ethene and terpenes (which are represented by equivalent CO emission in the original simulation) increases the emission rate of volatile organics from biogenic sources by 2% for ethene, 15% for terpenes.

2.3.1. Partitioning of Alkanes and Alkenes

[22] Summed $\geq$C4 alkanes in the original chemistry are divided into ALK4 (Butane + Pentane) and ALK7 (C6 and higher) for the extended chemistry, using the ratios of industrial emissions for ALK4 and ALK7 from *Atherton et al.* [1996]. Ethene, propene (a surrogate for externally bonded alkenes) and trans-2-butene (a surrogate for all internally bonded alkenes) in the extended chemistry are calculated from the single species propene (representing all alkenes) in the base chemistry using emission ratios from *Middleton et al.* [1990] for industrial emissions and from *Andreae and Merlet* [2001] for biomass burning emissions.

2.3.2. Aromatics

[23] Emissions for benzene, toluene (used to represent all benzene rings with additional carbon chains on one carbon of the benzene ring), and m-xylene (used to represent all benzene rings with additional carbon chains attached to two or more carbons of the ring) are generated from the total aromatics source developed by *Piccot et al.* [1992]. The ratios for benzene, toluene and m-xylene (25: 45: 30) are derived from field measurements of averaged local sources [*Goldan et al.*, 1995].

2.3.3. Biogenic Emissions of Terpenes and Ethene

[24] In the base chemistry, it is assumed that the monoterpene chemical life time is very short and quickly turns into a source of ethene (C_2H_4), which is used only to represent a biogenic source of CO from monoterpene oxidation [*Rodriguez et al.*, 2004]. For the extended chemistry, terpene emissions are divided into two surrogate species: alpha-pinene (67%) and limonene (33%) [*Griffin et al.*, 1999; *Atkinson and Arey*, 2003]. The contributions of individual compounds to emissions of monoterpenes on a global scale were inferred by *Griffin et al.* [1999]. Here, we used the estimates of *Griffin et al.* [1999] and assigned the individual compounds into alpha-pinene and limonene, on the basis of their lifetime for reaction with OH [*Atkinson and Arey*, 2003].

[25] The biogenic emissions of ethene were determined by scaling the isoprene flux, on the basis of work by *Goldstein et al.* [1996]. This study indicates emission ratios of ethene: propene: butene = 4: 2: 1 (on a molar basis), with total emissions of the alkenes approximately equal to 10% of the isoprene flux as in GMI [*Rodriguez et al.*, 2004].

2.3.4. Added Emissions From Biomass Burning

[26] The model with extended chemistry includes added emissions of phenol, formic acid and acetic acid from biomass burning. These emissions are not included in the model with base chemistry. Emissions from biomass burning were also added for methanol and acetone, as discussed below. Table 3 summarizes these values and also identifies changes relative to *Ito and Penner* [2004], on which they are based.

[27] The emissions from biomass burning are estimated separately as the sum of contributions from two sources: open vegetation burning and biofuel burning.

[28] Global emissions of phenol, formic acid and acetic acid from open vegetation burning in the extended model are set on the basis of estimates for the year 2000 from *Ito and Penner* [2004], modified by regional inverse model estimates for CO from *Arellano et al.* [2004]. Similar methods are used to derive emissions of methanol and acetone, as described in section 2.3.5. *Ito and Penner* [2004] provide estimates for geographically distributed emissions on a 1° by 1° grid. *Arellano et al.* [2004] provide estimates for emissions of CO from seven regions, including five regions with emissions dominated by open biomass burning. These inverse model estimates of CO are regarded as indicative of the total emissions source from open biomass burning and are used to correct for underestimates in burned areas which were found in the bottom-up estimate from *Ito and Penner* [2004] (see discussion by *Ito and Penner* [2005a, 2005b]). The emission estimates for each species from *Ito and Penner* [2004] are multiplied by a scaling factor equal to the ratio of regional CO emissions from *Arellano et al.* [2004] to the equivalent CO emissions from *Ito and Penner* [2004]. Some minor additional scaling was done to adjust for interannual and seasonal variability in emissions based on TOMS AI [*Herman et al.*, 1997; *Torres et al.*, 1998] as described by *Ito and Penner* [2005a], which is based on the work of *Duncan et al.* [2003].

[29] In the case of acetic acid, *Ito and Penner* [2004] provide a direct estimate for emissions. No direct estimate is available for formic acid or phenol. Formic acid emissions are derived from estimates for acetic acid emissions from *Ito and Penner* [2004], using ratios for formic acid to acetic acid emissions derived from *Andreae and Merlet* [2001] and *Bertschi et al.* [2003a]. The latter provide separate ratios for

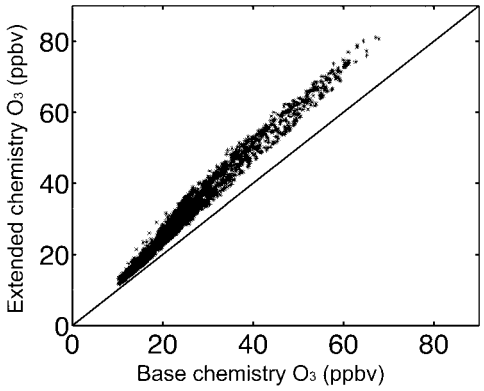

Figure 1. Scatter plot of O_3 in the simulations with base chemistry vs. extended chemistry. The plot shows monthly average O3 in ppb for July at 971 hPa. The solid line represents a 1-to-1 correspondence.

soil organic carbon (SOC) and coarse woody debris (CWD), which are used in combination with geographic information from *Ito and Penner* [2004] to obtain the total emission rate in each 1° by 1° grid. The resulting estimate for acetic acid is then scaled on the basis of CO emissions from *Arellano et al.* [2004] and adjusted for interannual and seasonal variability as described in the preceding paragraph. The same procedure is followed to derive emissions of phenol but its emissions are scaled to the methanol emissions by *Ito and Penner* [2004] rather than to acetic acid. A similar procedure is used for acetone (scaled to formaldehyde), as described in section 2.3.5.

[30] Emissions from biofuel burning for acetic acid and methanol are taken from *Ito and Penner* [2004] on the basis of the works of *Yevich and Logan* [2003] for the developing countries and the Food and Agricultural Organization Statistical Database, Rome, Italy, 2004 (available at http://faostat.fao.org) for the developed countries, using the emission factors from *Andreae and Merlet* [2001] and *Bertschi et al.* [2003b]. Emissions for acetone, formic acid, and phenol are scaled from the formaldehyde, acetic acid and methanol emissions given by *Ito and Penner* [2004], respectively.

2.3.5. Methanol and Acetone

[31] Emission rates for methanol and acetone were both used in the simulation with extended chemistry, but not in the simulation with base chemistry. In the case of acetone, the simulation with base chemistry used prescribed values instead of simulated values, and therefore included no emissions. In the case of methanol direct emissions were zero in the simulation with base chemistry.

[32] We used the geographic distribution of industrial emissions of C_3H_8 to derive the industrial emissions of methanol and acetone. The global totals were scaled to give a global source of 1.1 TgC yr^{-1} for methanol [*Singh et al.*, 2000] and 0.7 TgC yr^{-1} for acetone [*Jacob et al.*, 2002].

[33] We also scaled the geographic distribution of ocean emissions of CO [*Erickson*, 1989] to derive the ocean emissions of acetone. The total was scaled to give total ocean emissions of acetone equal to that of *Jacob et al.* [2002]. It is unclear whether the oceans actually represent a source for acetone, since air/sea flux measurements over the North Pacific Ocean indicate that the ocean is a net sink for acetone [*Marandino et al.*, 2005]. Further studies are needed to understand processes controlling ocean acetone levels near the air/sea interface and to quantify the temporal and spatial distribution of the net ocean flux.

[34] We scaled the geographic distribution of the isoprene flux to get the biogenic emissions of methanol and acetone. The totals were scaled to give a total biogenic source equal to the estimates of *Singh et al.* [2000] for methanol and *Jacob et al.* [2002] for acetone.

[35] Emissions from biomass burning were derived separately for open vegetation burning and for biofuels as described in section 2.3.4. Emissions of methanol from open vegetation burning were derived from direct estimates by *Ito and Penner* [2004] scaled to the CO emissions derived by *Arellano et al.* [2004] as described in section 2.3.4. Emissions of acetone from open vegetation burning and biofuels were scaled from estimates for formaldehyde. The same procedure for regional and monthly scaling is followed to derive monthly emissions of methanol and acetone on a 1° by 1° grid, as described in section 2.3.4. In addition, we adjusted the total emissions of acetone for biomass burning by scaling to the inverse results of *Jacob et al.* [2002], because of the large uncertainties in the emission factors of acetone and lack of measurements [*Andreae and Merlet*, 2001].

3. Results of Extended Chemistry

[36] Figures 1 through 7 show differences in monthly average species concentrations between the simulation with base chemistry and the simulation with extended chemistry. The differences between the two model versions are described here. Comparisons with measurements are shown in section 4.

3.1. Ozone (O_3)

[37] Ozone (Figures 1 and 2 and Table 4) increases by approximately 20% in the calculation with extended chemistry. As shown in Figure 1, the 20% increase in O_3 occurs in almost all locations at near-surface elevations. Similar percentage increases were found in the midtroposphere (see Table 4). This 20% change is comparable to the change calculated by *Pöschl et al.* [2000] in 0-D calculations, and somewhat larger than the change reported by *von Kuhlmann et al.* [2004].

[38] The most noticeable change in terms of magnitude is in industrially polluted regions and in regions with emissions from biomass burning. These regions include significant local photochemical production of O_3 in both the original simulation and the simulation with extended chemistry. The extended chemistry causes O_3 to increase by up to 15 ppb in these regions. Changes elsewhere in the troposphere are smaller in magnitude but represent a similar percentage increase, as shown in Figure 1. Percentage increases of O_3 are somewhat lower (10%) over the oceans, in the tropics and in the southern hemisphere.

[39] The major exception to this pattern occurs in the northern hemisphere (north of approximately 40°N latitude) during winter, where the increase in O_3 is 0 to 5% (see

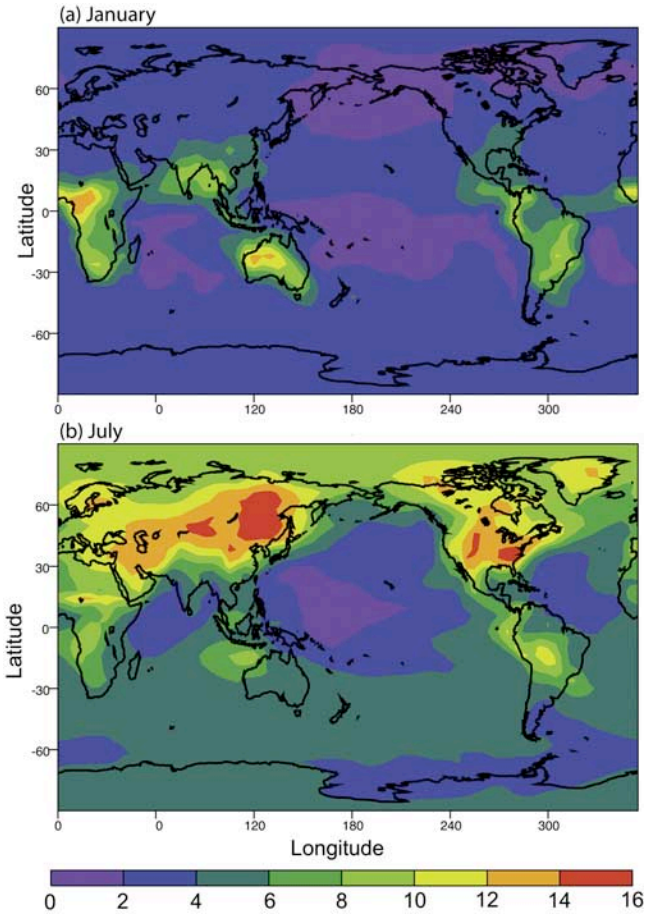

Figure 2. Change in monthly average O_3 associated with extended chemistry versus base chemistry. The plot shows the difference (in ppb) between O_3 in the model with extended chemistry and the model with base chemistry, for (a) January and (b) July at altitude 971 hPa. The scale extends from 0 to 16 ppb in increments of 2 ppb.

Table 4). A small region in the tropical western Pacific also has no increase in ozone (see Figure 2b).

[40] Two general factors are likely to contribute to the increased O_3 in the model with extended chemistry. The increase in VOC precursors can contribute directly to O_3 production in NO_x-saturated source regions and also in the NO_x-sensitive remote troposphere [*Jaeglé et al.*, 2001]. The second factor is a change in the distribution of NO_x, with increased transport of NO_x to the remote troposphere and also an overall increase in average NO_x concentrations (see section 3.3). This transport of NO_x to the remote troposphere increases overall production of O_3 because ozone production in the remote troposphere is more efficient [e.g., *Liu et al.*, 1987]. The increased VOC, increased overall NO_x and increased NO_x transport all result from the changes in chemistry and from the added VOC emissions in the extended model. This is described in detail in section 3.5.

3.2. OH and HO_2

[41] OH increases by approximately 10% in the simulation with extended chemistry (see Figure 3 and Table 4). Increased OH is found in most of the troposphere, except in source regions dominated by anthropogenic emissions and in northern locations during winter. The 10% increase occurs throughout the free troposphere. At the surface the 10% increase is found over most of the oceans, and somewhat larger increases are found over forested land regions. A few surface locations have OH increased by 50% or more, including parts of the Amazon and central African rain forests, northern Australia, and northern Canada during July. HO_2 shows little change throughout most of the troposphere. The ratio OH/HO_2 also increases.

[42] The increase in OH and in the OH/HO_2 ratio is associated with the increase in NO_x in most of the troposphere, in the simulation with enhanced photochemistry. The largest photochemical sources of OH in the remote troposphere are the reaction of NO with HO_2 and the photolysis of O_3. Both NO and O_3 increase in the simulation with enhanced photochemistry. The largest increases in OH are found in tropical continental locations with high biogenic emissions, very low NO_x and low emissions from anthropogenic sources. In these locations the production of alkyl nitrates from isoprene in the extended model and their subsequent reaction to release NO_x can have a large impact on the ambient NO_x concentration, which in turn affects OH. The changed isoprene chemistry also results in higher concentrations of organic precursors of radicals and of O_3 in these regions, which contributes to the increased OH.

Table 4. Model Concentrations: Zonal Average at 36–40 N for Model With Base and Extended Chemistry[a]

	O_3		OH		NO_x		PAN	
Altitude, hpa	Base	Ext.	Base	Ext.	Base	Ext.	Base	Ext.
				July				
990.	33.6	40.9	0.0727	0.0778	0.687	0.670	0.112	0.218
700.	50.5	59.8	0.173	0.1918	0.0725	0.0868	0.113	0.216
500.	65.7	76.5	0.182	0.203	0.0461	0.055	0.279	0.444
300.	84.9	97.7	0.199	0.215	0.0954	0.109	0.296	0.470
				January				
990.	39.1	41.1	0.0157	0.0160	1.12	1.04	0.333	0.465
700.	50.9	52.4	0.0175	0.0173	0.0254	0.0261	0.175	0.244
500.	56.9	58.5	0.0215	0.0209	0.0198	0.0199	0.162	0.232
300.	90.4	89.3	0.0459	0.0464	0.0583	0.0568	0.147	0.213

[a]Results are in ppt for OH and ppb for other species.

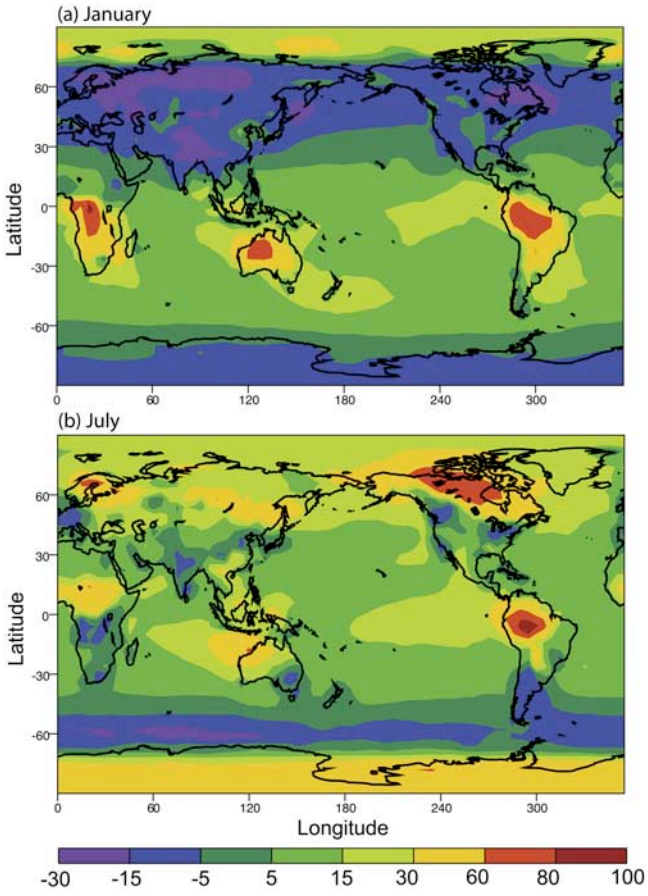

Figure 3. Change in monthly average OH associated with extended chemistry versus base chemistry. The plot shows the difference between OH in the model with extended chemistry and the model with base chemistry, expressed as a percentage of the value in the model with base chemistry, for (a) January and (b) July at altitude 971 hPa.

3.3. Reactive Nitrogen

[43] The change in NO_x associated with extended chemistry (Figure 4 and Table 4) shows a pattern marked by decreased concentrations in source regions in the northern hemisphere, especially in winter, and significant increases in the remote troposphere. The increases are most notable in remote northern locations in summer, including locations that lie downwind from NOx source regions. The largest magnitude increases in NO_x are found in the northern Atlantic Ocean (downwind from North America) and the northwest Pacific Ocean (downwind from source regions in Asia). High-percentage increases in NO_x also appear downwind from regions with significant biomass burning. NO_x is increased by 20% or more over much of the Atlantic and Pacific oceans, in both hemispheres, during both summer and winter. NO_x also increases by 20% (global average) in the midtroposphere. By contrast, NO_x decreases by approximately 10% in northern hemisphere source regions, including much of the U.S., Europe and China. NO_x also decreases in some remote locations in the tropics, especially over the western tropical Pacific Ocean, and in the north polar region in winter. The decrease in NO_x in source regions is smaller in absolute terms than the increase in remote locations and in the free troposphere, and the total NO_x content of the troposphere increases by 10% in the extended model.

[44] Nitric acid (HNO_3) increases by approximately 15% over much of the troposphere in the simulation with extended chemistry, both near the surface and at in the midtroposphere. The 15% increase in HNO_3 appears uniformly over most ocean regions. Because HNO_3 is formed directly from NO_x and has a relatively long lifetime, the change in HNO_3 reflects the average change in ambient NO_x. HNO_3 decreases by approximately 20% over most continental regions, reflecting the omission of direct production of HNO_3 from isoprene in the simulation with extended chemistry. Wet and dry deposition of HNO_3 represents the dominant removal mechanism for reactive nitrogen in both versions of the model, and the increased rate of removal of HNO_3 over the oceans in the extended version is balanced by the decreased rate of removal over the continents.

[45] Peroxyacetyl nitrate (PAN) is one of the most significant species because of its impact on the transport of NOx [e.g., *Singh and Hanst*, 1981; *Singh et al.*, 1998, 2000;

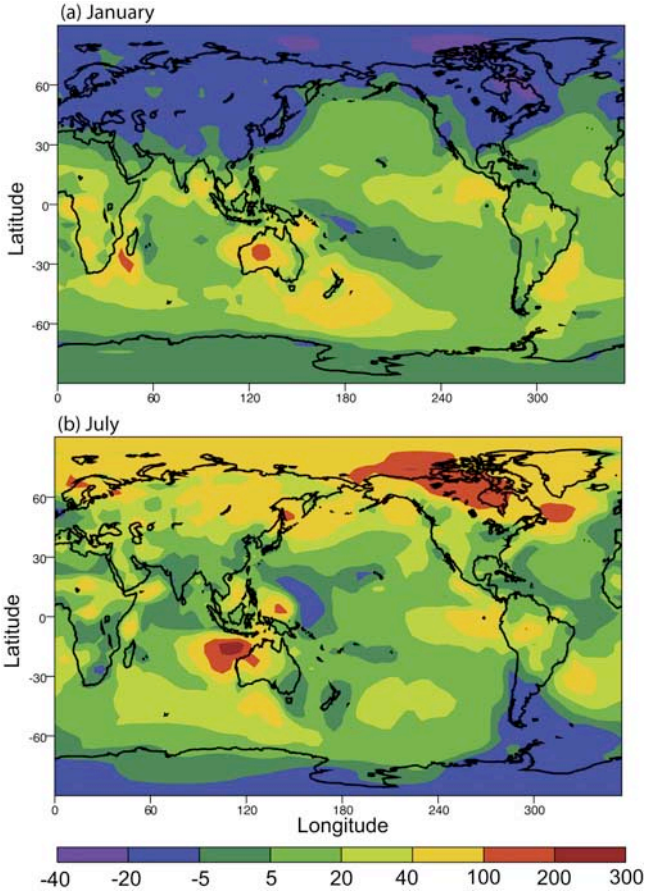

Figure 4. Change in monthly average NO_x associated with extended chemistry versus base chemistry. The plot shows the difference between NO_x in models with extended chemistry and the model with base chemistry, expressed as a percentage of the value in the model with base chemistry, for (a) January and (b) July at altitude 971 hPa.

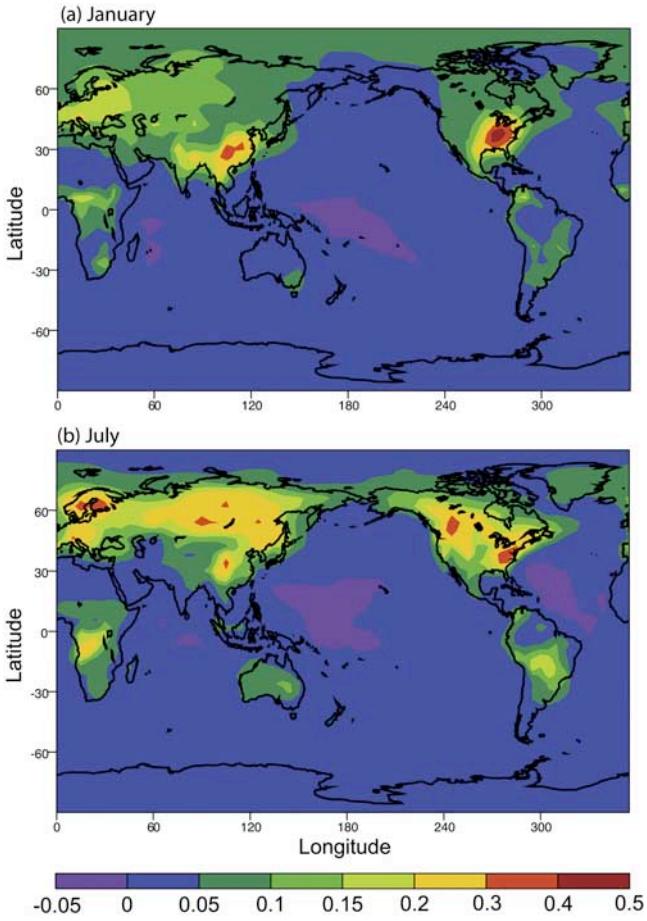

Figure 5. Change in monthly average PAN associated with extended chemistry versus base chemistry. The plot shows the difference (in ppb) between PAN in the model with extended chemistry versus the model with base chemistry, for (a) January and (b) July at altitude 971 hPa.

Schultz et al., 1999; *Horowitz and Jacob*, 1999; *Wang et al.*, 1998b]. Results from the simulation with extended chemistry show 20–30% higher PAN over large regions at the surface, mainly over the continents (Figure 5). Changes are much smaller near the surface over the oceans and in the southern hemisphere in general (except near regions with emissions from biogenic sources or biomass burning). A small decrease in PAN occurs in parts of the tropical Pacific Ocean. At the midtroposphere (not shown) the 20–30% increase in PAN extends more widely and includes most of the northern hemisphere north of 30°. In contrast with the results for O_3 and NO_x, the simulation with extended chemistry also has increased PAN at northern locations during winter (see Table 4). In terms of absolute magnitude the change in PAN is highest in polluted regions, but in percentage terms the increase in PAN extends over most of the troposphere.

[46] Isoprene nitrates account for as much as 20% of total reactive nitrogen in source regions in the model with enhanced photochemistry. Isoprene nitrates reach concentrations as high as 1 ppb in regions with high emissions of both isoprene and NO_x, such as the southern U.S. during summer. Isoprene nitrate concentrations are small outside of source regions. Peroxymethacryloyl nitrate ($CH_2 = CCH_3CO_3NO_2$), a species produced from the degradation of isoprene with PAN-like properties, is typically present at concentrations equal to 20% of the PAN concentration in isoprene source regions. Organic nitrates associated with alpha-pinene generally account for 5% of reactive nitrogen or less, even in regions with high emission of alpha-pinene.

3.4. Other Organics

[47] Changes in primary organics (alkanes and alkenes) generally reflect the changes in chemistry between the original and extended versions. Summed $\geq$C4 alkanes are decreased by 40% throughout the troposphere in the simulation with extended chemistry. This is a direct result of the more rapid removal rate in the extended chemistry, which includes a separate tracer for shorter-lived higher alkanes. Similarly, summed $\geq$C3 alkenes decrease by 40% in the simulation with extended chemistry, as a result of the inclusion of *trans*-2-butene as a surrogate for internally bonded alkenes. The original simulation used propene, a less reactive species, as a surrogate for all alkenes.

[48] Among the secondary organics, the major differences between the original and extended chemistry involve methyl glyoxal ($CH_3C(O)CHO$) and hydroxyacetone ($HOCH_2C(O)CH_3$). Ambient concentrations of methyl glyoxal are increased by a factor of two, and hydroxyacetone by a factor of three in the simulation with extended chemistry. Hydroxyacetone concentrations in the midtroposphere reach 100 ppt in the simulation with extended chemistry, a magnitude comparable to that of acetone. Methyl glyoxal reaches 10 ppt in the midtroposphere, which is significant because of its high reactivity. Significant changes in ambient concentrations also occur for acetone, methanol, formic and acetic acids and peroxypropional nitrate. These changes are discussed in relation to model measurement comparisons below (section 4).

[49] Summed VOC reactivity increases by up to 20% in the simulation with extended photochemistry. VOC reactivity here is defined as the sum of concentrations of each individual VOC species (excluding CO and CH_4) multiplied by the rate constant for its reaction with OH. The increased VOC reactivity is most notable in source regions and includes contributions from the added aromatics and terpenes and their reaction products. Increased VOC reactivity is smaller (10% or less) in the remote troposphere, where reactivity is dominated by the products of CH_4 oxidation (formaldehyde and methyl peroxide).

3.5. Discussion of Photochemistry

[50] As discussed in section 3.1, the increased O_3 in the extended simulation is due in part to the direct impact of increased VOC on ozone formation rates and in part to the effect of changed NO_x concentrations. The chemistry that drives these changes is discussed here.

[51] On the basis of an off-line calculation, rates of formation of odd oxygen (defined here as the sum of O_3 and NO_2) increase by10–20% in the extended simulation, both in source regions and in the remote troposphere. The off-line analysis consists of calculated rates of photochemical production and loss based on monthly average concentrations in each model grid. Although the percentage

increases are similar, the controlling factors are different in source regions as opposed to the remote troposphere.

[52] Source regions usually have a significant (20%) increase in reactivity-weighted VOC in the extended model. Depending on location and season, the increased VOC can be due to either the added aromatics and other anthropogenic species, terpenes, or the inclusion of hydroxyalkyl nitrate production from isoprene. Off-line calculations show that model O_3 in these regions increases with increasing NO_x and with increasing VOC. NO_x is often lower in these regions in the extended simulation, but the effect of reduced NO_x on ozone formation is more than compensated by the effect of increased VOC. In the free troposphere and in remote regions rates of ozone formation also increase with both NO_x and VOC, but here the increased ozone formation in the extended simulation is due primarily to the increased NO_x. NO_x increases in the extended simulation are usually much larger on a percentage basis than increases in VOC in the free troposphere and have a larger impact on ozone formation.

[53] The change in NO_x between the base and extended simulations is due to two different factors. NO_x decreases in source regions and increases in the remote troposphere as a result of more efficient transport associated with PAN and its higher-order homologues. Total NO_x in the troposphere also increases, largely as a result of the recycling of NO_x from hydroxyalkyl nitrates associated with isoprene and terpenes. NO_x increases by 20% in most of the remote troposphere and by 10% in the troposphere as a whole, suggesting that transport of NO_x and recycling of NO_x from PAN-like compounds are equally responsible for the increased O_3.

[54] The peroxyacetyl radical (the immediate precursor of PAN) has five major photochemical precursors: acetaldehyde (CH_3CHO); acetone (CH_3COCH_3); methylethylketone ($C_2H_5COCH_3$) and other similar ketones; methyl glyoxal ($CH_3C(O)CHO$) and hydroxyacetone ($HOCH_2C(O)CH_3$). The simulation with extended chemistry has significantly increased concentrations of methyl glyoxal and hydroxyacetone (by factors of 2 or more) and minor increases in the other precursors. The increased rate of PAN formation can be attributed to these species. The off-line calculation suggests that hydroxyacetone is especially important as a precursor of peroxyacetyl radicals. Hydroxyacetone typically represents 5% of reactivity-weighted VOC but provides up 50% of the photochemical source of peroxyacetyl radicals (either directly or following conversion to methyl glyoxal).

[55] Hydroxyacetone in the extended chemistry is produced from double-bonded organics, including isoprene and the alpha-pinenes. The photochemistry in the extended model includes a high yield of hydroxyacetone from the reactions of hydroxyalkyl nitrates associated with isoprene and terpenes. These nitrates are a major source of the increased hydroxyacetone in the extended model. Methyl glyoxal is produced from the reaction products of isoprene (including hydroxyacetone) and from aromatics. Hydroxyacetone and aromatics both contribute to the increased methyl glyoxal in the extended model.

[56] Production of alkyl-nitrate-like species from isoprene in the model with extended chemistry instead of direct production of HNO_3 has the effect of increasing both PAN formation and ambient NO_x in source regions. The nitrates produced from isoprene are assumed to deposit rapidly in the model (at a rate similar to HNO_3), but this deposition is not instantaneous. On the basis of the reaction rate of these species with OH (3.2×10^{-11} molec^{-1} cm^{-3} s^{-1}, from *Treves and Rudich* [2003]), photochemical removal occurs on a timescale of a few hours, which is more rapid than removal by dry deposition from a daytime convective mixed layer. Consequently, most of the nitrogen content of these species is rereleased into the atmosphere as NO_x rather than removed by deposition. The photochemical reaction of these isoprene nitrates also releases organics which subsequently contribute to the formation of hydroxyacetone. By contrast, isoprene peroxy radicals react with NO to form HNO_3 in the original photochemical representation. This represents an effective sink for both NO_x and organics, because the reactions of HNO_3 to rerelease NO_x are much slower than the process of deposition.

[57] The rerelease of NO_x from organic nitrates may explain why ambient NO_x does not decrease (and sometimes even increases) in source regions that also have high emissions of biogenics. The increased formation rate of PAN in the simulation with extended chemistry would otherwise lead to reduced ambient NO_x. Ambient NO_x is reduced in source regions of the northern hemisphere during winter (when biogenic emissions are negligible), but during the northern summer and in source regions in the tropics the increased rate of PAN formation is compensated by rerelease of NO_x from isoprene nitrates.

[58] *Pöschl et al.* [2000], *von Kuhlmann et al.* [2004], and *Fiore et al.* [2005] also report that the formation of isoprene nitrates leads to an increase in global O_3, and *Horowitz et al.* [1998] attributed the impact of isoprene emissions on O_3 largely to the effect of isoprene nitrates. The predicted impact here is somewhat larger than that given by *von Kuhlmann et al.* [2004] and *Fiore et al.* [2005]. This may be due to the production of hydroxyacetone from isoprene nitrates in our mechanism, which follows *Paulson and Seinfeld* [1992], in contrast to the production of the shorter-lived hydroxyacetaldehyde in the mechanisms used by *von Kuhlmann et al.* [2004] and *Fiore et al.* [2005].

4. Model Measurement Comparisons

[59] Figures 6–12 show monthly average species concentrations from the simulations with original and extended photochemistry in comparison with a compilation of ambient measurements from field campaigns developed by *Emmons et al.* [2000], and with methanol from *Singh et al.* [2000, 2001].

[60] *Emmons et al*. [2000] analyzed measurements of various species and calculated statistics over several regions during field campaigns. The data set provides effective vertical profiles of measured species, including both the mean and standard deviation of measurements made within the selected regions. This data has been widely used to evaluate chemistry/transport models [e.g., *Bey et al.*, 2001; *Rotman et al.*, 2004]. Here, we show comparisons between the data compilation by *Emmons et al*. [2000] and results from both the original simulation and the simulation with extended chemistry, in order to identify whether the changes in the extended chemistry simulation affect the agreement between models and measurements.

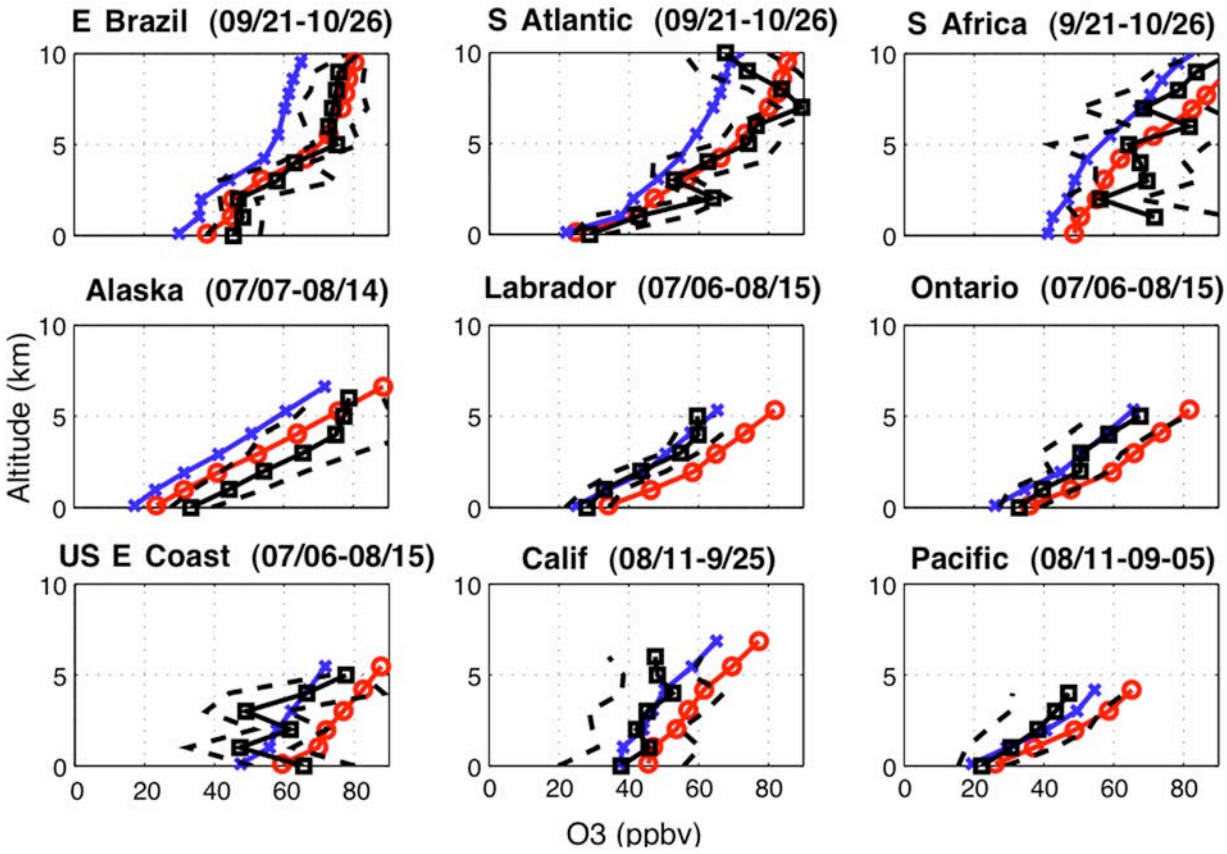

Figure 6. Comparison between measured O_3 in ppb and model results at various sites. The black squares represent the average of measurements over the selected regions and the periods of date reported by *Emmons et al.* [2000]. The dashed lines show the standard deviations of measured values. The red line and circles represents the model with extended chemistry. The blue line and X's represents the model with base chemistry.

4.1. O_3, NO_x and PAN

[61] Figures 6 and 7 compare the mean modeled O_3 and PAN profiles with measurements at various sites. O_3 and PAN are associated with the most noticeable difference between results for the original and extended photochemistry. As shown in the figures, O_3 is increased by 20% and PAN by up to 40% in the simulation with extended photochemistry. Despite this difference, there is no clear evidence of bias in the model measurement comparisons for either simulation.

[62] There is no clear evidence of bias in part because the range of ambient measurements identified by *Emmons et al.* [2000] typically includes variations of greater than 20% for O_3 and greater than 40% for PAN. A 20–40% change in model ambient concentrations, while potentially significant in itself, is hard to evaluate versus ambient measurements. Referring to Figure 6, it can be seen that the model with extended chemistry shows significantly better agreement with measured O_3 at some sites (e.g., Brazil) and significantly worse at others (e.g., Labrador). Generally, the model with base chemistry underestimates O_3 in the tropics, while the model with extended chemistry overestimates O_3 at northern midlatitudes during summer. This regional pattern may be due in part to differences between the specific model year (1997) and measurement ensembles for a multiyear period. PAN (Figure 7) is also overestimated at many northern midlatitude sites during summer in the model with extended chemistry, while PAN is underestimated at tropical and southern hemisphere sites in the model with base chemistry. In general, the model measurement comparison for PAN shows a tendency to overestimate, which is somewhat worse for the model with extended photochemistry. However, the comparison with measured PAN also shows some locations with significant model underestimates, which are improved in the simulation with extended photochemistry. It cannot be easily judged whether the effects on O_3 and PAN are improved or not, because some sites are improved, some sites are degraded, and others do not change very much.

[63] To test this further, we have applied a linear least squares regression to the ensemble of ozonesonde measurements identified by *Logan* [1999] in comparison with monthly average O_3 from model results for both base and extended chemistry. We also derived regression statistics for model versus measured PAN, using the ensemble of measurements identified by *Emmons et al.* [2000]. Results (Table 5) show little preference for either model version. Correlation coefficients are similar for both models. The

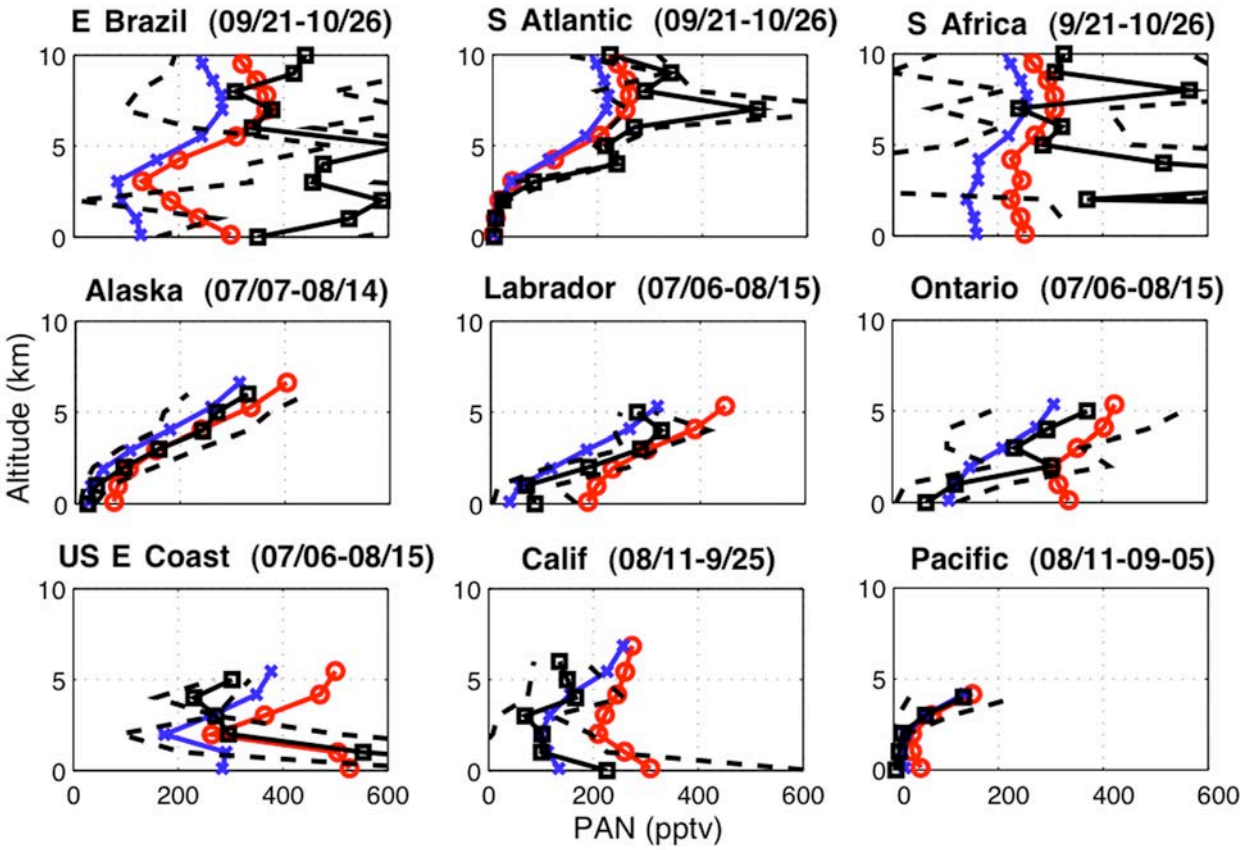

Figure 7. Comparison between measured PAN in ppt and model results at various sites. Symbols and lines are as in Figure 6.

regression slope is significantly lower than unity and intercepts are large, suggesting that both models tend to overestimate the lowest values and underestimate the highest values. Similarly, the standard deviations of the measured ensembles are higher than the standard deviations of the equivalent ensembles of model values. The ensemble mean O_3 is 5% low relative to observations for the model with base chemistry and 7% high for the model with extended chemistry. In the case of PAN, the ensemble mean is closer to the observed mean for the model with base chemistry (13% low) than for the model with extended chemistry (43% high), but given the low correlation coefficients, we do not regard this as firm evidence in favor of the base chemistry. The level of statistical agreement is slightly worse than reported by *von Kuhlmann et al.* [2003a, 2003b].

[64] With regard to NO_x (Figure 8), the model with extended chemistry results in 10–20% higher concentrations throughout the troposphere. Comparisons with measurements assembled by *Emmons et al.* [2000] generally show model measurement agreement to within a factor of 2. Model measurement agreement is slightly worse for the model with extended chemistry (e.g., at the Ontario site). However, the day-to-day variation in measured values (±50% at most sites) make it difficult to derive conclusive evidence from the difference between the two models.

4.2. Peroxypropionylnitrate (PPN)

[65] Peroxypropionylnitrate (PPN) is decreased by a factor of two or more in the simulation with extended chemistry at remote sites (see Figure 9). The precursor of PPN, summed >C2 aldehydes, is also decreased by a factor of two.

[66] The reduced PPN occurs because PPN was effectively used as a surrogate for other higher-order PAN-like species in the original chemistry of Evans et al. (2003). Formation of PPN in the base chemistry included reaction pathways from the photochemical decomposition of the various hydroxyalkyl peroxides. These account for more than 50% of PPN production in the base chemistry. In the extended mechanism hydroxyalky peroxides no longer produce >C2 aldehydes (leading to formation of PPN). Instead, they are assumed to produce glycolaldehyde, methyl glyoxal and hydroxyacetone, which have been identified as reaction products of the parent species (see section 2.2). PPN in the extended mechanism is still used as a surrogate for other PAN-like species, but these include only the directly analogous species produced from higher-order alkanes.

[67] As a result, PPN in the extended mechanism can be effectively compared to direct measurements of PPN. The model reproduces the very low PPN (<1 ppt) observed at several sites in the southern hemisphere. However, the model overestimates PPN by a factor of five or more at

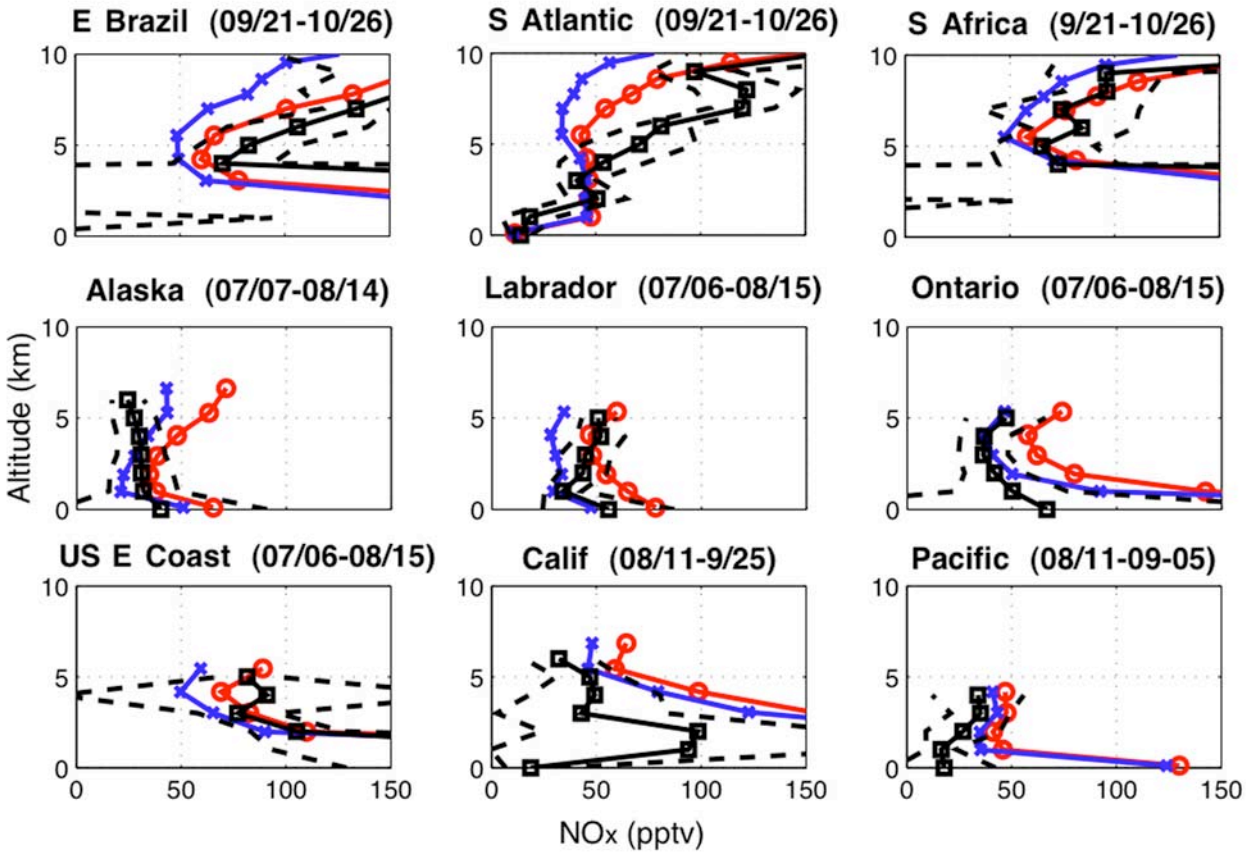

Figure 8. Comparison between measured NO_x in ppt and model results at various sites. Symbols and lines are as in Figure 6.

two sites (Ireland, Newfoundland) that are influenced by outflow from polluted continental regions.

[68] The ratio PPN/PAN has been reported from several studies in the U.S. [e.g., *Pippin et al.*, 2001; *Thornberry et al.*, 2001; *Nouaime et al.*, 1998; *Roberts et al.*, 1998]. *Pippin et al.* [2001] report PPN/PAN ratios of 0.1 at a rural site in the northern U.S. during summer, increasing to 0.2 during winter/spring. The simulation with enhanced chemistry shows similar PPN/PAN ratios and similar seasonal behavior.

4.3. Acetone

[69] Acetone (CH_3COCH_3) was set to a prescribed value in the original simulation. In the simulation with extended chemistry the prescribed acetone is replaced with a full calculation based on photochemical production, loss and transport. As shown in Figure 10, the calculated acetone shows good agreement with ambient measurements, with the exception of Labrador, the U.S. east coast and east Atlantic sites. The model measurement agreement is as good for calculated acetone as it was for the prescribed values. Because acetone contributes significantly to the upper tropospheric HO_x budget through photolysis [*Singh et al.*, 1995; *McKeen et al.*, 1997; *Collins et al.*, 1999; *Müller and Brasseur*, 1999; *Jaeglé et al.*, 2001], this comparison is especially significant.

4.4. Methanol

[70] Results for methanol (CH_3OH) differ greatly between the original and extended simulations because the extended simulation includes direct emissions of methanol. Potentially large direct emissions of methanol associated with biomass burning have been suggested by *Singh et al.* [2000], *Galbally and Kirstine* [2002], and *Ito and Penner* [2004]. Based on these findings 100 Tg/yr methanol were directly injected in the simulation with extended chemistry using the inventory developed by *Ito and Penner* [2004] with adjustments described above in section 2.3.5. The original simulation did not contain direct emission of methanol. Photochemical source strengths of methanol are similar in the two simulations (44 Tg/yr in the base simulation versus 46 Tg/yr in the simulation with extended photochemistry), but the photochemical source is smaller than the direct emission of methanol in the latter simulation. Ambient concentrations of methanol (Figure 11) are significantly higher in the simulation with extended chemistry, as a result of the added direct emissions.

[71] As shown in Figure 11, the addition of direct emission of methanol generally results in improved agreement with measurements [*Singh et al.*, 2000, 2001]. The original simulation underestimated methanol by a factor of two in comparison with measurements at sites throughout the Pacific Ocean. This underestimate is largely (though not entirely) eliminated in the simulation with extended chem-

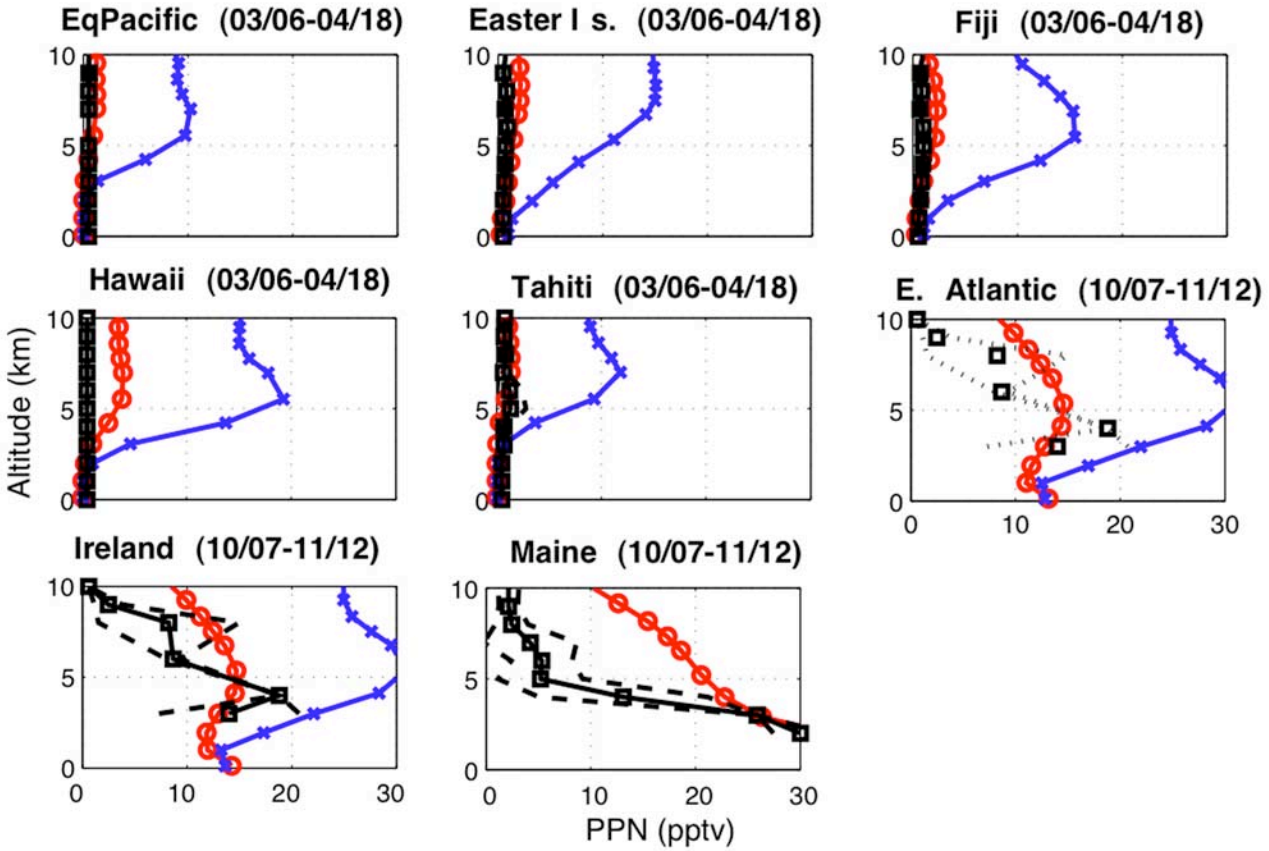

Figure 9. Comparison between measured peroxypropional nitrate (PPN) in ppt and model results at various sites. Symbols and lines are as in Figure 6.

istry. Evidence from sites in and near the Atlantic Ocean is less clear. The original simulation also underestimated methanol in comparison with measurements at all three Atlantic sites, while the simulation with extended chemistry overestimates methanol at two of the three sites (most notably at Ireland, where model values exceed measured values by a factor of two).

[72] Because of a long life time against wet deposition (120 days) [*Jacob et al.*, 2005] and its minor contribution to total loss (7%) [*von Kuhlmann et al.*, 2003b], wet deposition does not significantly affect the vertical profile of methanol in the troposphere [*Crutzen and Lawrence*, 2000]. The results shown here are based on simulations with zero wet deposition of methanol. These show good overall agreement with measured values, and the variation of methanol with height in the model agrees with measurements.

[73] The sources of methanol in the simulation with extended chemistry (100 Tg/yr from emissions, 47 Tg/yr from photochemical production) are significantly higher than the methanol sources calculated by *von Kuhlmann et al.* [2003b] (77 Tg/yr from emissions, 28 Tg/yr from photochemical production).

4.5. Formic and Acetic Acids

[74] Formic acid (HCOOH) is produced from the ozonolysis of alkenes, terpenes and some isoprene reaction products in the extended chemistry model, and by the reactions of CH_3CO_3 radical with some peroxy radicals. The direct emissions (10 Tg/yr) and the photochemical source (17 Tg/yr) in the extended chemistry still result in underestimates compared to the observations at most sites (Figure 12). The direct emission source of formic acid used here is lower than the source used by *von Kuhlmann et al.* [2003b] (17 Tg/yr), while the photochemical source is somewhat larger than *von Kuhlmann*'s [2003b] (14 Tg/yr).

[75] Acetic acid (CH_3COOH) is photochemically produced in the model mainly from the reactions of the CH_3CO_3 radical with HO_2 and with organic peroxy radicals. The total photochemical source is 38 and 42 Tg/yr for the base and extended chemistry simulations, respectively. These values are considerably smaller than those calculated by *von Kuhlmann et al.* [2003b] (75 Tg/yr) and by *Baboukas et al.* [2000] (120 Tg/yr), although the same reaction rate constant was used here for the $CH_3CO_3 + HO_2$ reaction as in the work of *von Kuhlmann et al.* [2003b], following the recommendation of *Tyndall et al.* [2001]. The lower rate of photochemical production may be due to our inclusion of the reactions of CH_3CO_3 with all RO_2 radicals, including those produced from isoprene and its products. These reactions (with product yields from Evans et al. (2003) based on the work of *Tyndall et al.* [2001]) also produce acetic acid but with yields (10%) that are lower than the yields of the competing reactions of CH_3CO_3 with HO_2 (yield 50%) and with CH_3O_2 (yield 40%).

[76] Comparison with aircraft measurements over the Atlantic and Pacific shows that the mixing ratios of acetic

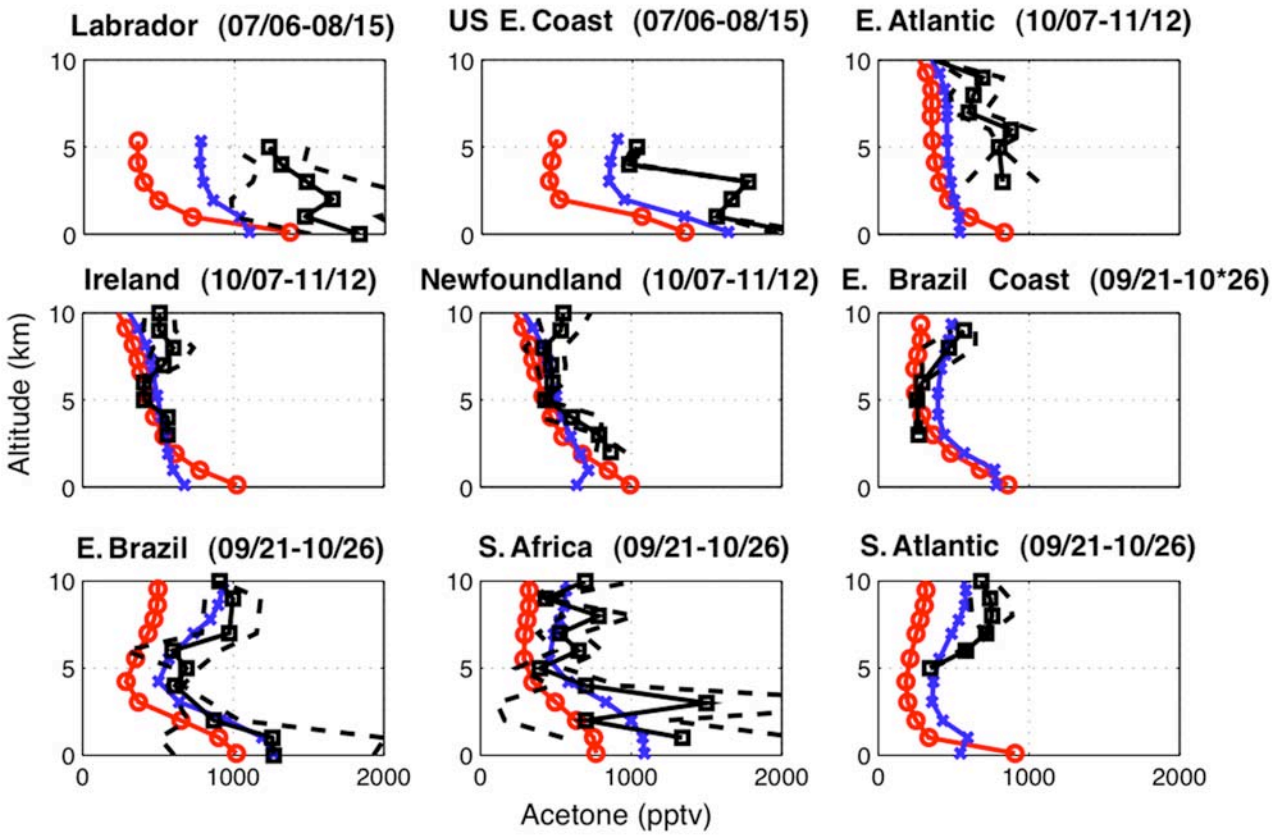

Figure 10. Comparison between measured acetone in ppt and model results at various sites. Symbols and lines are as in Figure 6. Acetone in the model with base chemistry (blue lines) represents prescribed values.

acid can be either over or underestimated by the model with extended chemistry, but are generally overestimated by the original model (Figure 13). The higher calculated values in the original simulation are probably due to the lack of deposition in the Harvard/GMI treatment of acetic acid. Deposition accounts for almost 50% of the total removal of acetic acid in the model with extended chemistry.

4.6. Isoprene Nitrates, Hydroxyacetone, and Other Biogenic Reaction Products

[77] The addition of alkyl nitrates and similar species produced from isoprene has a major impact on results from the simulation with enhanced chemistry (see section 3.5). Ambient isoprene nitrates in the model reached as high as 1 ppb during summer in regions such as the eastern U.S., which combine high isoprene emissions with high anthropogenic NO_x. The isoprene nitrates accounted for approximately 20% of total reactive nitrogen (NO_y). These levels of isoprene nitrates are much higher than have been found in specific measurements of individual alkyl nitrates [e.g., *Thornberry et al.*, 2001]. However, *Day et al.* [2003] measured alkyl nitrates as an ensemble sum at a rural site in California and found that the summed alkyl nitrates and related species reach as high as 500 ppt and represent 20% of NO_y. The measurements reported by *Day et al.* are consistent with results from the model with extended chemistry over North America.

[78] The products of isoprene oxidation, including hydroxyacetone and methyl glyoxal, also have a significant impact on photochemistry in the model (see section 3.5). Hydroxyacetone in the model reaches 100 ppt in the midtroposphere and reaches 1 ppb near the surface in source regions. Surface measurements of hydroxyacetone have found 0.61 ppb in Surinam [*Williams et al.*, 2001] and 0.38 ppb in an isoprene-rich forest in California [*Spaulding et al.*, 2003]. Although these measured values are somewhat lower than model ambient values they suggest that the model values are not unreasonable. However, *Grossmann et al.* [2003] measured 0.16 ppb hydroxyacetone in Germany, much lower than the model value there (1.2 ppb).

[79] A comparison between model results and measured reactive nitrogen and isoprene reaction products reported by *Day et al.* [2003] and *Spaulding et al.* [2003] is shown in Table 6. This comparison must be viewed with caution because the measured values were influenced by local geographical features cannot be simulated with the coarse grid resolution of the model. The measurement site (Blodgett Forest, CA, at 38°53′N, 120°37′W) was located in the foothills of the Sierra Nevada mountains, whereas the model grid encompassing the site included agricultural plains and urbanized areas as well. In particular, the good agreement between model results and measured primary species at the site (NO_x and isoprene) should be regarded as a coincidence.

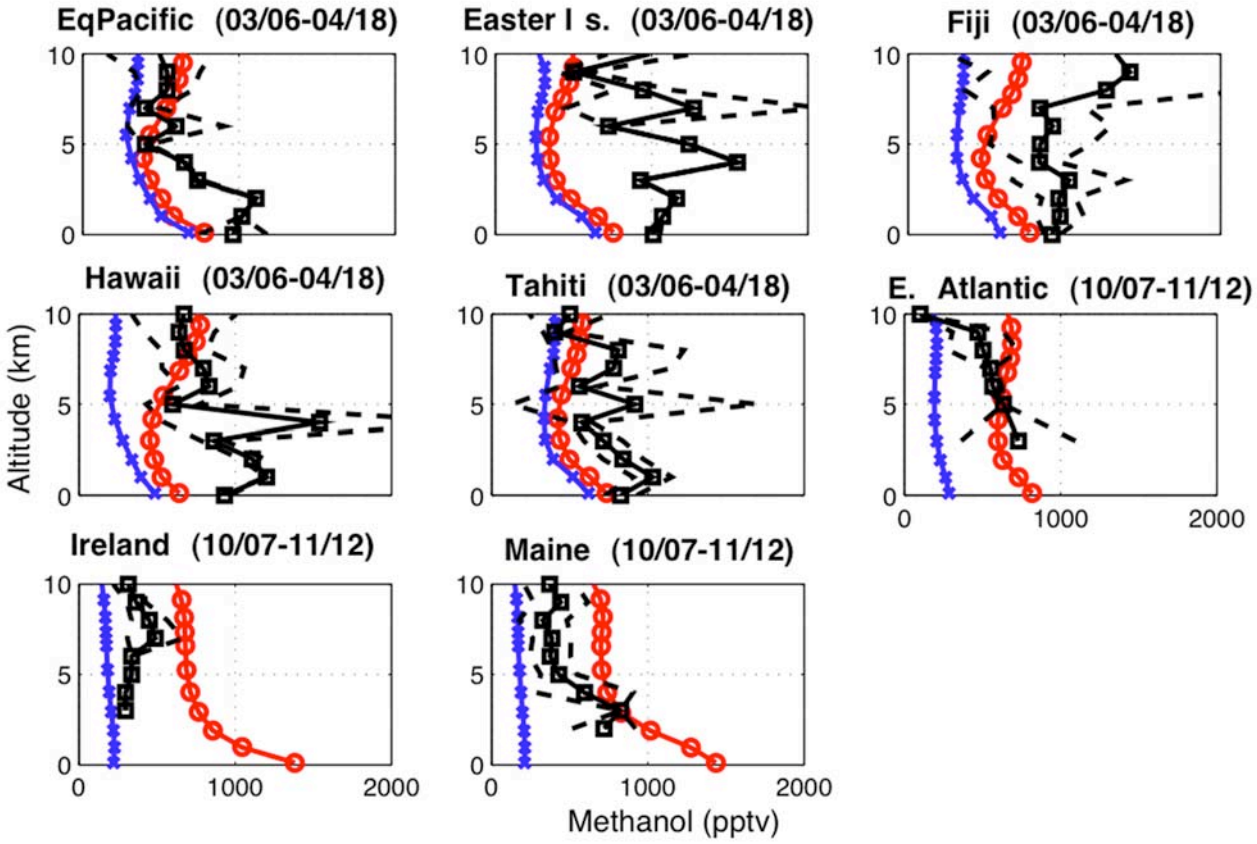

Figure 11. Comparison between measured methanol in ppt and model results at various sites. Symbols and lines are as in Figure 6. Measurements are from *Singh et al.* [2000, 2001].

[80] The extended model shows reasonable values for the summed alkyl nitrates, although its values are lower than the measured median. The ratio of alkyl nitrates to summed PAN were also somewhat lower than the ratio of median measured values, and the ratio of alkyl nitrates to HNO_3 was comparable to the ratio of median measured values. This represents a significant improvement over the model with base chemistry, which underestimated alkyl nitrates by an order of magnitude.

[81] Hydroxyacetone in the extended model exceeded the median measured value by nearly a factor of two, while hydroxyacetone in the model with base chemistry was lower than the measured median by a factor of two. Glycolaldehyde in the extended model was lower than the measured median by a factor of two (though within the range of measured values), while glycolaldehyde in the base model was lower than the measured median by an order of magnitude. Methyl glyoxal was comparable to the measured median in the extended model and lower than the measured median by a factor of two in the base model. The other reaction products of isoprene, including methylvinyl ketone, methacrolein and acetone, were lower than the median measured values by approximately a factor of two in both the extended and base models. The model values for all species fell within the range of measured values at the site, with the exception of the alkyl nitrates and glycolaldehyde, which were below the minimum measured value in the base model.

[82] On the basis of median values alone, the hydroxyacetone in the extended model appears reasonable. However, the ratio between hydroxyacetone and other isoprene reaction products (methylvinyl ketone and methacrolein) in the extended model is higher than the ratio of median measured values by factors of five and four respectively. Ratios between methyl glyoxal and methylvinyl ketone and between methyl glyoxal and methacrolein are also higher than the ratio of measured median values by a factor of two. The ratios for hydroxyacetone and methyl glyoxal are closer to the ratio of measured medians in the base model. In addition, the ratio of methacrolein to methylvinyl ketone in the extended model is significantly higher than the ratio of measured medians. This ratio is close to the measured ratio in the base model.

[83] These comparisons provide support for two features of the extended chemistry: inclusion of alkyl nitrates produced from isoprene and the subsequent reaction of alkyl nitrates to produce glycolaldehyde. The evidence for hydroxyacetone and methyl glyoxal is less clear, but the comparison suggests that these species are overestimated in the extended model.

5. Conclusions

[84] A model for global-scale gas-phase photochemistry and transport has been exercised with extended representation of both emissions and photochemistry. The extended

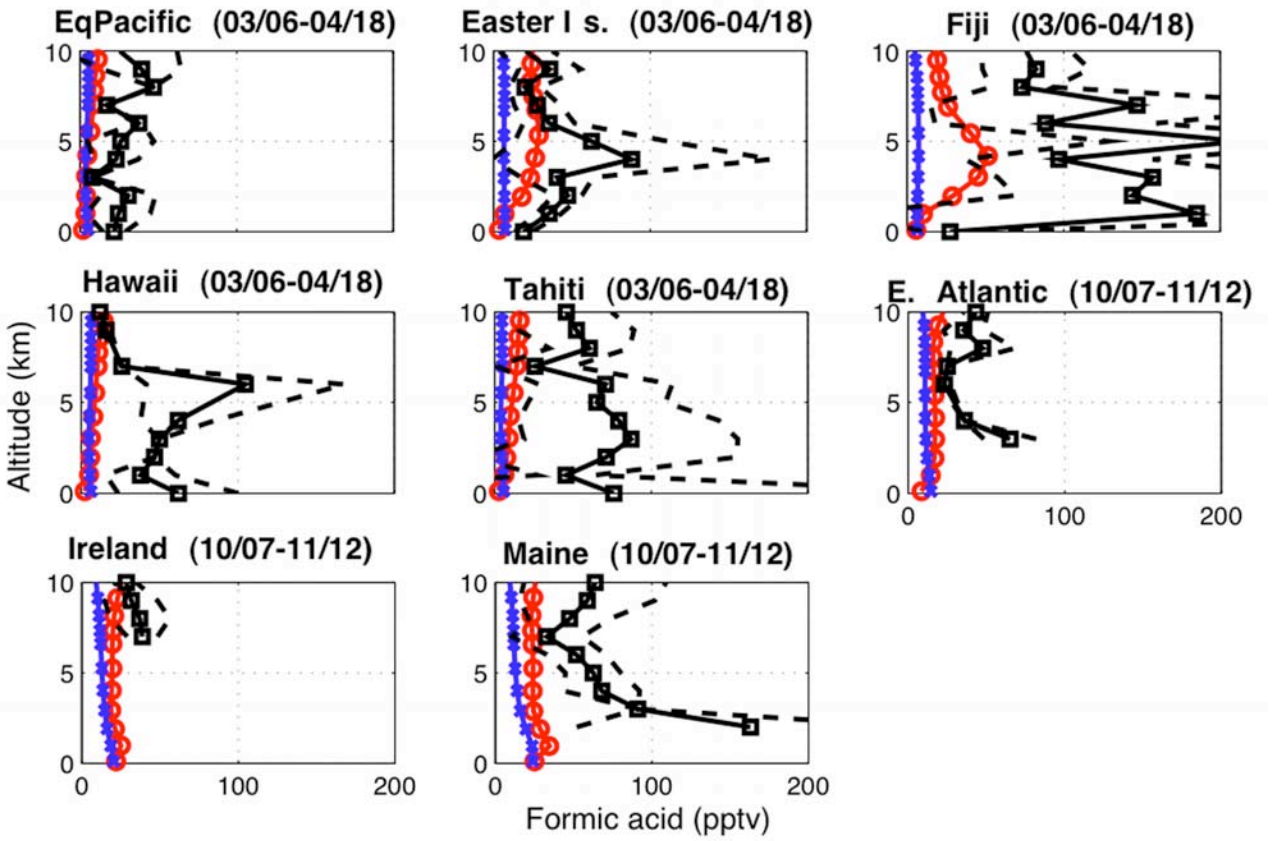

Figure 12. Comparison between measured formic acid in ppt and model results at various sites. Symbols and lines are as in Figure 6.

representation includes emission and photochemistry of aromatic and terpenoid hydrocarbons and explicit representation of alkyl-nitrate-like species produced by the reaction of NO with isoprene, methylvinylketone and methacrolein. Other modifications include calculated rather than prescribed values of acetone and the addition of direct emissions of methanol, phenol, acetic acid and formic acid associated with biomass burning, along with biogenic emission of methanol.

[85] The model extensions resulted in a 20% increase in calculated model values for O_3, a 40% increase in PAN and a 10% increase in the OH radical. The increase in O_3 and OH were driven by the increased rate of formation of PAN, which has the effect of transporting NO_x from source regions to the free troposphere. NO_x in the free troposphere was increased by approximately 20%. The isoprene nitrates had an important effect on model photochemistry because they reacted to release both NO_x and organics. The increased NO_x leads directly to increased ozone formation, especially in the free troposphere where ozone production efficiency per NO_x is higher. Similar findings have been reported by *Pöschl et al.* [2000], *von Kuhlmann et al.* [2004], and *Fiore et al.* [2005].

[86] The increased formation rate of PAN was associated with increased concentration of two PAN precursors: methyl glyoxal and hydroxyacetone. These species are formed by the photochemical oxidation of aromatics, isoprene and alpha-pinene, and in particular from the breakdown of the isoprene nitrates.

[87] Model results for O_3 and PAN showed reasonable agreement with an ensemble of ambient measurements, but the model measurement comparison did not provide con-

Table 5. Correlation Between Model and Observed O_3 and PAN[a]

		Observations		Base Chemistry					Extended Chemistry				
Species	N	Mean	S.D.	Mean	S.D.	m	b	r^2	Mean	S.D.	m	b	r^2
O_3	4267	56	28	53	19	0.55	21	0.63	60	21	0.60	27	0.63
PAN	330	.129	.196	.112	.096	0.28	0.076	0.33	.143	.129	0.40	0.092	0.37

[a]The table shows results for model monthly average O_3 and PAN in comparison with the ensemble of measured O_3 from *Logan* [1999] and measured PAN from *Emmons et al.* [2000] for models with base chemistry and extended chemistry. This includes slope (m) and intercept (b) for a least squares linear regression ($X_m = a*X_{obs} + b$, for model concentrations X_m and observed X_{obs} in ppb), correlation coefficient (r^2), number of observations (N), mean and standard deviation (S.D.).

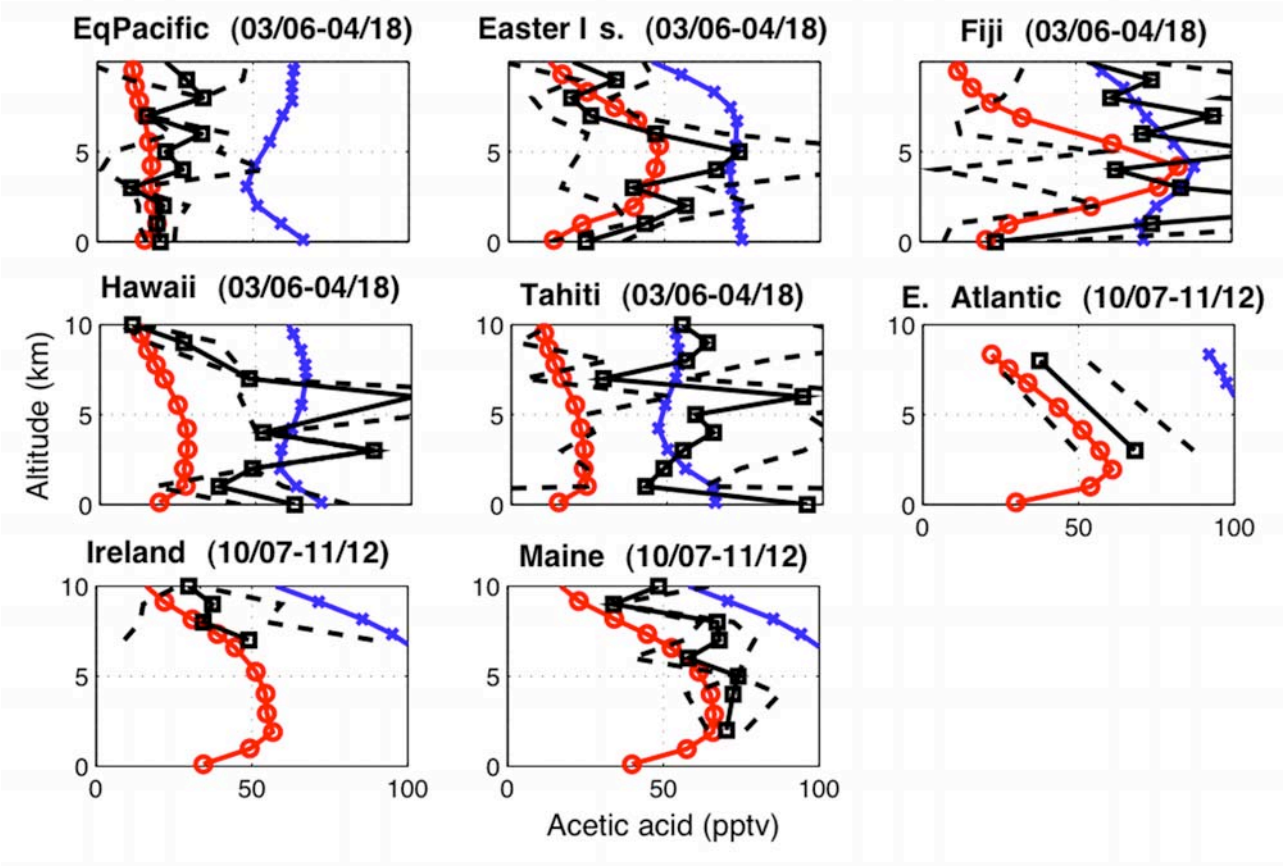

Figure 13. Comparison between measured acetic acid in ppt and model results at various sites. Symbols and lines are as in Figure 6.

clusive evidence concerning the increased O_3 and PAN in the extended model. Model measurement agreement for O_3 and PAN was equally good with and without the model extensions. The measured values of O_3 and PAN included variations of 50% or more, and model measurement discrepancies at individual sites also exceeded 50%. The size of the change in model O_3 and PAN was too small to evaluate effectively with measurements. A limited comparison with measured alkyl nitrates suggested that the ambient concentrations in the model with extended chemistry were reasonable. The model overestimates hydroxyacetone in comparison with measured values, suggesting that subsequent reactions of the hydroxyalkyl nitrates associated with isoprene lead to the production of glycolaldehye rather than hydroxyacetone. Future simulations will explore this possi-

Table 6. Model versus Measured Values at Blodgett Forest, California[a]

Species	Measured Range, ppb	Measured Median, ppb	Base Model, ppb	Extended Model, ppb
Reactive nitrogen	[*Day et al.*, 2003]			
NO_x	0.1–2.0	0.8	1.3	1.1
HNO_3	0.3–2.1	1.2	1.1	1.0
Peroxyacetyl nitrates (PANs)	0.2–1.5	0.8	0.19	0.40
Alkyl nitrates	0.1–1.4	0.5	0.03	0.16
Other organics	[*Spaulding et al.*, 2003]			
Isoprene	0.01–2.4	0.43	0.33	0.33
Methylvinyl ketone	0.01–1.7	0.54	0.16	0.16
Methacrolein	0.02–0.83	0.36	0.12	0.18
Glycolaldehyde	0.09–1.7	0.63	0.06	0.30
Hydroxyacetone	0.08–1.1	0.38	0.16	0.68
Glyoxal	0.006–0.08	0.02	0.01	0.01
Methyl glyoxal	0.03–0.32	0.12	0.05	0.12
Acetone	0.22–4.6	2.2	1.1	0.78

[a]Measured reactive nitrogen (including organic nitrates) are median values from *Day et al.* [2003]. Measured nonnitrate organics are the median and range of values from *Spaulding et al.* [2003]. Model results are from the simulations with base chemistry and with extended chemistry for August. All results are in ppb.

bility and will likely lead to smaller increases in PAN and O_3 in the extended model.

[88] Model measurement comparisons also showed reasonable agreement for acetone, methanol, and formic and acetic acids. The model measurement agreement for methanol provides some measure of validation for the estimated emissions from biomass burning and biogenic sources [*Ito and Penner*, 2005a], which were included in the extended chemistry. The model measurement comparison for peroxypropional nitrate was significantly improved by the removal of the reaction pathway that produced peroxypropional nitrate from the breakdown of hydroxyalkly peroxides from biogenic sources.

[89] **Acknowledgments.** Support for this research was provided by a grant to J. Penner from the Atmospheric Chemistry Program of the Department of Energy and by grants 0207841 and 0454838 to S. Sillman from the National Science Foundation. Any opinions, findings, and conclusions or recommendations expressed in this material are those of the authors and do not necessarily reflect the views of the National Science Foundation. Support was also provided by the NASA Atmospheric Chemistry Modeling and Analysis Program, award NNG05GD29G.

References

Andreae, M. O., and P. Merlet (2001), Emission of trace gases and aerosols from biomass burning, *Global Biogeochem. Cycles*, *15*, 955–966.

Arellano, A. F., Jr., P. S. Kasibhatla, L. Giglio, G. R. van der Werf, and J. T. Randerson (2004), Top-down estimates of global CO sources using MOPITT measurements, *Geophys. Res. Lett.*, *31*, L01104, doi:10.1029/2003GL018609.

Atherton, C. S., and J. E. Penner (1988), The transformation of nitrogen oxides in the polluted troposphere, *Tellus, Ser. B*, *40*, 380–392.

Atherton, C. S., S. Grotch, D. D. Parrish, J. E. Penner, and J. J. Walton (1996), The role of anthropogenic emissions of NO_x on tropospheric ozone over the North Atlantic Ocean: A three-dimensional, global model study, *Atmos. Environ.*, *30*, 1739–1751.

Atkinson, R., and J. Arey (2003), Atmospheric degradation of volatile organic compounds, *Chem. Rev.*, *103*, 4605–4639.

Atkinson, R., D. L. Baulch, R. A. Cox, J. N. Crowley, R. F. Hampson, R. G. Hynes, M. E. Jenkin, M. J. Rossi, and J. Troe (2004), Evaluated kinetic and photochemical data for atmospheric chemistry: Volume 1–gas phase reactions of O_x, HO_x, NO_x, and SO_x, species, *Atmos. Chem. Phys.*, *4*, 1461–1738.

Baboukas, E. D., M. Kanakidou, and N. Mihalopoulos (2000), Carboxylic acids in gas and particulate phase above the Atlantic Ocean, *J. Geophys. Res.*, *105*, 14,459–14,471.

Balkanski, Y. J., D. J. Jacob, G. M. Gardner, W. C. Graustein, and K. K. Turekian (1993), Transport and residence times of tropospheric aerosols inferred from a global three-dimensional simulation of ^{210}Pb, *J. Geophys. Res.*, *98*, 20,573–20,586.

Bertschi, I., R. J. Yokelson, D. E. Ward, R. E. Babbitt, R. A. Susott, J. G. Goode, and W. M. Hao (2003a), Trace gas and particle emissions from fires in large diameter and belowground biomass fuels, *J. Geophys. Res.*, *108*(D13), 8472, doi:10.1029/2002JD002100.

Bertschi, I. T., R. J. Yokelson, D. E. Ward, T. J. Christian, and W. M. Hao (2003b), Trace gas emissions from the production and use of domestic biofuels in Zambia measured by open-path Fourier transform infrared spectroscopy, *J. Geophys. Res.*, *108*(D13), 8469, doi:10.1029/2002JD002158.

Betterton, E. A., and M. R. Hoffmann (1988), Henry's law constants of some environmentally important aldehydes, *Environ. Sci. Technol.*, *22*, 1415–1418.

Bey, I., et al. (2001), Global modeling of tropospheric chemistry with assimilated meteorology: Model description and evaluation, *J. Geophys. Res.*, *106*, 23,073–23,096.

Briegleb, B. P. (1992), Delta-Eddington approximation for solar radiation in the NCAR community climate model, *J. Geophys. Res.*, *97*, 7603–7612.

Carter, W. P. L. (2000), Documentation of the SAPRC-99 chemical mechanism for VOC reactivity assessment, final report to the California Air Resources Board, *Rep. 00-AP-RT17-001-FR*, May 8 , Air Pollut. Res. Cent., Coll. Eng., Cent. Environ. Res. Technol., Univ. of Calif., Riverside.

Collins, W. J., D. S. Stevenson, C. E. Johnson, and R. G. Derwent (1999), Role of convection in determining the budget of odd hydrogen in the upper troposphere, *J. Geophys. Res.*, *104*, 26,927–26,941.

Coy, L., and R. Swinbank (1997), Characteristics of stratospheric winds and temperatures produced by data assimilation, *J. Geophys. Res.*, *102*, 25,763–25,781.

Coy, L., E. R. Nash, and P. A. Newman (1997), Meteorology of the polar vortex: Spring 1997, *Geophys. Res. Lett.*, *24*, 2693–2696.

Crutzen, P. J., and M. G. Lawrence (2000), The impact of precipitation scavenging on the transport of trace gases: A 3-dimensional model sensitivity study, *J. Atmos. Chem.*, *37*, 81–112.

Day, D. A., M. B. Dillon, P. J. Wooldridge, J. A. Thornton, R. S. Rosen, E. C. Wood, and R. C. Cohen (2003), On alkyl nitrates, O_3, and the "missing NO_y", *J. Geophys. Res.*, *108*(D16), 4501, doi:10.1029/2003JD003685.

Duncan, B. N., R. V. Martin, A. C. Staudt, R. Yevich, and J. A. Logan (2003), Interannual and seasonal variability of biomass burning emissions constrained by satellite observations, *J. Geophys. Res.*, *108*(D2), 4100, doi:10.1029/2002JD002378.

Emmons, L. K., et al. (1997), Climatologies of NO_x and NO_y: A comparison of data and models, *Atmos. Environ.*, *31*, 1851–1904.

Emmons, L. K., D. A. Hauglustaine, J.-F. Müller, M. A. Carroll, G. P. Brasseur, D. Brunner, J. Staehelin, V. Thouret, and A. Marenco (2000), Data composites of airborne observations of tropospheric ozone and its precursors, *J. Geophys. Res.*, *105*, 20,497–20,538.

Erickson, D. J., III (1989), Ocean to atmosphere carbon monoxide flux: Global inventory and climate implications, *Global Biogeochem. Cycles*, *3*, 305–314.

Feng, Y., J. E. Penner, S. Sillman, and X. Liu (2004), Effects of cloud overlap in photochemical models, *J. Geophys. Res.*, *109*, D04310, doi:10.1029/2003JD004040.

Fiore, A. M., L. W. Horowitz, D. W. Purves, H. Levy II, M. J. Evans, Y. Wang, Q. Li, and R. M. Yantosca (2005), Evaluating the contribution of changes in isoprene emissions to surface ozone trends over the eastern United States, *J. Geophys. Res.*, *110*, D12303, doi:10.1029/2004JD005485.

Galbally, I. E., and W. Kirstine (2002), The production of methanol by flowering plants and the global cycle of methanol, *J. Atmos. Chem.*, *43*, 195–229.

Giorgi, F., and W. L. Chameides (1986), Rainout lifetimes of highly soluble aerosols and gases as inferred from simulations with a general circulation model, *J. Geophys. Res.*, *91*, 14,367–14,376.

Goldan, P. D., M. Trainer, W. C. Kuster, D. D. Parish, J. Carpenter, J. M. Roberts, J. E. Yee, and F. C. Fehsenfeld (1995), Measurements of hydrocarbons, oxygenated hydrocarbons, carbon monoxide, and nitrogen oxides in an urban basin in Colorado: Implications for emission inventories, *J. Geophys. Res.*, *100*, 22,771–22,783.

Goldstein, A. H., S. M. Fan, M. L. Goulden, J. W. Munger, and S. C. Wofsy (1996), Emissions of ethene, propene, and *1*-butene by a mid-altitude forest, *J. Geophys. Res.*, *101*, 9149–9157.

Griffin, R., D. Cocker III, J. Seinfeld, and D. Dabdub (1999), Estimate of global atmospheric organic aerosol from oxidation of biogenic hydrocarbons, *Geophys. Res. Lett.*, *26*, 2721–2724.

Grossmann, G., et al. (2003), Hydrogen peroxide, organic peroxides, carbonyl compounds, and organic acids measured at Pabstthum during BERLIOZ, *J. Geophys. Res.*, *108*(D4), 8250, doi:10.1029/2001JD001096.

Herman, J. R., P. K. Bhartia, O. Torres, C. Hsu, C. Seftor, and E. Celarier (1997), Global distribution of UV-absorbing aerosols from Nimbus-7/TOMS data, *J. Geophys. Res.*, *102*, 16,911–16,922.

Horowitz, L., J. Liang, G. Gardner, and D. Jacob (1998), Export of reactive nitrogen from North America during summertime: Sensitivity to hydrocarbon chemistry, *J. Geophys. Res.*, *103*, 13,451–13,476.

Horowitz, L. W., and D. J. Jacob (1999), Global impact of fossil fuel combustion on atmospheric NO_x, *J. Geophys. Res.*, *104*, 23,823–23,840.

Houweling, S., F. Dentener, and J. Lelieveld (1998), The impact of nonmethane hydrocarbon compounds on tropospheric photochemistry, *J. Geophys. Res.*, *103*, 10,673–10,696.

Ito, A., and J. E. Penner (2004), Global estimates of biomass burning emissions based on satellite imagery for the year 2000, *J. Geophys. Res.*, *109*, D14S05, doi:10.1029/2003JD004423.

Ito, A., and J. E. Penner (2005a), Historical emissions of carbonaceous aerosols from biomass and fossil fuel burning for the period 1870–2000, *Global Biogeochem. Cycles*, *19*, GB2028, doi:10.1029/2004GB002374.

Ito, A., and J. E. Penner (2005b), Estimates of CO emissions from open biomass burning in southern Africa for the year 2000, *J. Geophys. Res.*, *110*, D19306, doi:10.1029/2004JD005347.

Jacob, D. J., S. Sillman, J. A. Logan, and S. C. Wofsy (1989), Least independent variables method for simulation of tropospheric ozone, *J. Geophys. Res.*, *94*, 8497–8509.

Jacob, D. J., B. D. Field, E. M. Jin, I. Bey, Q. Li, J. A. Logan, R. M. Yantosca, and H. B. Singh (2002), Atmospheric budget of acetone, *J. Geophys. Res.*, *107*(D10), 4100, doi:10.1029/2001JD000694.

Jacob, D. J., et al. (2005), Global budget of methanol: Constraints from atmospheric observations, *J. Geophys. Res.*, *110*, D08303, doi:10.1029/2004JD005172.

Jaeglé, L., D. J. Jacob, W. H. Brune, and P. O. Wennberg (2001), Chemistry of HO_x radicals in the upper troposphere, *Atmos. Environ.*, *35*(3), 469–489.

Johnson, B. J., E. A. Betterton, and D. Craig (1996), Henry's law coefficients of formic and acetic acids, *J. Atmos. Chem.*, *24*, 113–119.

Kasibhatla, P. S., H. Levy II, and W. J. Moxim (1993), Global NO_x, HNO_3, PAN, and NO_y distributions from fossil fuel combustion emissions: A model study, *J. Geophys. Res.*, *98*, 7165–7180.

Lide, D. R. (Ed.) (1999), *CRC Handbook of Chemistry and Physics*, 80th ed., CRC Press, Boca Raton, Fla.

Liu, S. C., M. Trainer, F. C. Fehsenfeld, D. D. Parrish, E. J. Williams, D. W. Fahey, G. Hubler, and P. C. Murphy (1987), Ozone production in the rural troposphere and the implications for regional and global ozone distributions, *J. Geophys. Res.*, *92*, 4191–4207.

Liu, H., D. J. Jacob, I. Bey, and R. M. Yantosca (2001), Constraints from ^{210}Pb and ^{7}Be on wet deposition and transport in a global three-dimensional chemical tracer model driven by assimilated meteorological fields, *J. Geophys. Res.*, *106*, 12,109–12,128.

Liu, X., and J. E. Penner (2002), Effect of Mount Pinatubo H_2SO_4/H_2O aerosol on ice nucleation in the upper troposphere using a global chemistry and transport model, *J. Geophys. Res.*, *107*(D12), 4141, doi:10.1029/2001JD000455.

Liu, X., J. E. Penner, and M. Herzog (2005), Global modeling of aerosol dynamics: Model description, evaluation, and interactions between sulfate and non-sulfate aerosols, *J. Geophys. Res.*, *110*, D18206, doi:10.1029/2004JD005674.

Logan, J. A. (1999), An analysis of ozonesonde data for the troposphere: Recommendations for testing 3-D models and development of a gridded climatology for tropospheric ozone, *J. Geophys. Res.*, *104*, 16,115–16,149.

Lurmann, F. W., A. C. Lloyd, and R. Atkinson (1986), A chemical mechanism for use in long-range transport/acid deposition computer modeling, *J. Geophys. Res.*, *91*, 10,905–10,936.

Marandino, C. A., W. J. De Bruyn, S. D. Miller, M. J. Prather, and E. S. Saltzman (2005), Oceanic uptake and the global atmospheric acetone budget, *Geophys. Res. Lett.*, *32*, L15806, doi:10.1029/2005GL023285.

Mari, C., D. J. Jacob, and P. Bechtold (2000), Transport and scavenging of soluble gases in a deep convective cloud, *J. Geophys. Res.*, *105*, 22,255–22,267.

McKeen, S. A., T. Gierczak, J. B. Burkholder, P. O. Wennberg, T. F. Hanisco, E. R. Keim, R.-S. Gao, S. C. Liu, A. R. Ravishankara, and D. W. Fahey (1997), The photochemistry of acetone in the upper troposphere: A source of odd-hydrogen radicals, *Geophys. Res. Lett.*, *24*, 3177–3180.

McLinden, C., S. Olsen, B. Hannegan, O. Wild, M. Prather, and J. Sundet (2000), Stratospheric ozone in 3-D models: A simple chemistry and the cross-tropopause flux, *J. Geophys. Res.*, *105*, 14,653–14,666.

Middleton, P., W. R. Stockwell, and W. P. L. Carter (1990), Aggregation and analysis of volatile organic compound emissions for regional modeling, *Atmos. Environ., Part A*, *24*, 1107–1133.

Müller, J.-F., and G. Brasseur (1999), Sources of upper tropospheric HO x: A three-dimensional study, *J. Geophys. Res.*, *104*, 1705–1715.

Nouaime, G., et al. (1998), Sequential oxidation products from tropospheric isoprene chemistry: MACR and MPAN at a NO_x-rich forest environment in the southeastern United States, *J. Geophys. Res.*, *103*, 22,463–22,472.

O'Sullivan, D. W., M. Lee, B. C. Noone, and B. G. Heikes (1996), Henry's law constant determinations for hydrogen peroxide, methyl hydroperoxide, hydroxymethyl hydroperoxide, ethyl hydroperoxide, and peroxyacetic acid, *J. Phys. Chem.*, *100*, 3241–3247.

Paulson, S. E., and J. H. Seinfeld (1992), Development and evaluation of a photooxidation mechanism for isoprene, *J. Geophys. Res.*, *97*, 20,703–20,715.

Penner, J. E., C. S. Atherton, J. Dignon, S. J. Ghan, J. J. Walton, and S. Hameed (1991), Tropospheric nitrogen: A three-dimensional study of sources, distributions, and deposition, *J. Geophys. Res.*, *96*, 959–990.

Penner, J. E., D. J. Bergmann, J. J. Walton, D. Kinnison, M. J. Prather, D. Rotman, C. Price, K. E. Pickering, and S. L. Baughcum (1998), An evaluation of upper troposphere NO_x with two models, *J. Geophys. Res.*, *103*, 22,097–22,113.

Piccot, S. D., J. J. Watson, and J. W. Jones (1992), A global inventory of volatile organic compound emissions from anthropogenic sources, *J. Geophys. Res.*, *97*, 9897–9912.

Pippin, M. R., S. Bertman, T. Thornberry, M. Town, M. A. Carroll, and S. Sillman (2001), Seasonal variation of PAN, PPN, MPAN and O_3 at the upper Midwest PROPHET site, *J. Geophys. Res.*, *106*, 24,451–24,463.

Pöschl, U., R. von Kuhlmann, N. Poisson, and P. J. Crutzen (2000), Development and intercomparison of condensed isoprene oxidation mechanisms for global atmospheric modeling, *J. Atmos. Chem.*, *37*, 29–52.

Prather, M., et al. (2003), Fresh air in the 21st century?, *Geophys. Res. Lett.*, *30*(2), 1100, doi:10.1029/2002GL016285.

Régimbal, J. M., and M. Mozurkewich (1997), Peroxynitric acid decay mechanisms and kinetics at low pH Source, *J. Phys. Chem.*, *101*, 8822–8829.

Roberts, J. M., et al. (1998), Measurements of PAN, PPN, and MPAN made during the 1994 and 1995 Nashville Intensives of the Southern Oxidants Study: Implications for regional ozone production from biogenic hydrocarbons, *J. Geophys. Res.*, *103*, 22,473–22,490.

Rodriguez, J. M., B. N. Duncan, J. A. Logan, B. Das, J. Kouatchou, and S. E. Strahan (2004), The budget of ozone and its precursors as calculated by the Global Modeling Initiative, *Eos Trans. AGU*, *85*(47), Fall Meet. Suppl., Abstract A51G-03.

Rotman, D. A., et al. (2004), IMPACT, the LLNL 3-D global atmospheric chemical transport model for the combined troposphere and stratosphere: Model description and analysis of ozone and other trace gases, *J. Geophys. Res.*, *109*, D04303, doi:10.1029/2002JD003155.

Sander, R., et al. (2003), Chemical kinetics and photochemical data for use in atmospheric studies, Evaluation number 14, *JPL Publ. 02-25*, 334 pp.

Schultz, M. G., et al. (1999), On the origin of tropospheric ozone and NO_x over the tropical South Pacific, *J. Geophys. Res.*, *104*, 5829–5844.

Schwartz, S. E., and W. H. White (1981), Solubility equilibria of the nitrogen oxides and oxyacids in dilute aqueous solution, in *Advances in Environmental Science and Engineering*, edited by J. R. Pfafflin and E. N. Ziegler, vol. 4, pp. 1–45, Gordon and Breach, New York.

Shepson, P. B., E. Mackay, and K. Muthuramu (1996), Henry's law constants and removal processes for several atmospheric β-hydroxy alkyl nitrates, *Environ. Sci. Technol.*, *30*, 3618–3623.

Sillman, S. (1991), A numerical solution to the equations of tropospheric chemistry based on an analysis of sources and sinks of odd hydrogen, *J. Geophys. Res.*, *96*, 20,735–20,744.

Singh, H. B. (1987), Reactive nitrogen in the troposphere, *Environ. Sci. Tech.*, *21*, 320–327.

Singh, H. B., and P. L. Hanst (1981), Peroxyacetyl Nitrate (PAN) in the unpolluted atmosphere: An important reservoir for nitrogen oxides, *Geophys. Res. Lett.*, *8*, 941–944.

Singh, H. B., M. Kanakidou, P. J. Crutzen, and D. J. Jacob (1995), High concentrations and photochemical fate of oxygenated hydrocarbons in the global troposphere, *Nature*, *378*, 50–54.

Singh, H. B., et al. (1998), Latitudinal distribution of reactive nitrogen in the free troposphere over the Pacific Ocean in late winter/early spring, *J. Geophys. Res.*, *103*, 28,237–28,247.

Singh, H., et al. (2000), Distribution and fate of selected oxygenated organic species in the troposphere and lower stratosphere over the Atlantic, *J. Geophys. Res.*, *105*, 3795–3806.

Singh, H. B., Y. Chen, A. C. Staudt, D. J. Jacob, D. R. Blake, B. G. Heikes, and J. Snow (2001), Evidence from the Pacific troposphere for large global sources of oxygenated organic compounds, *Nature*, *410*, 1078–1081.

Spaulding, R. S., R. W. Talbot, and M. J. Charles (2002), Optimization of a mist chamber (cofer scrubber) for sampling water-soluble organics in air, *Environ. Sci. Technol.*, *36*(8), 1798–1808.

Spaulding, R. S., G. W. Schade, A. H. Goldstein, and M. J. Charles (2003), Characterization of secondary atmospheric photo-oxidation products: Evidence for biogenic and anthropogenic sources, *J. Geophys. Res.*, *108*(D8), 4247, doi:10.1029/2002JD002478.

Staudinger, J., and P. V. Roberts (1996), A critical review of Henry's law constants for environmental applications, *Critical Rev. Environ. Sci. Technol.*, *26*, 205–297.

Stockwell, W. R., F. Kirchner, M. Kuhn, and S. Seefeld (1997), A new mechanism for regional atmospheric chemistry modeling, *J. Geophys. Res.*, *102*, 25,847–25,880.

Thornberry, T. D., et al. (2001), Observations of reactive oxidized nitrogen and speciation of NO_y during PROPHET summer 1998, *J. Geophys. Res.*, *106*, 24,359–24,386.

Torres, O., P. K. Bhartia, J. R. Herman, Z. Ahmad, and J. Gleason (1998), Derivation of aerosol properties from satellite measurements of backscattered ultraviolet radiation: Theoretical basis, *J. Geophys. Res.*, *103*, 17,099–17,110.

Treves, K., and T. Rudich (2003), The atmospheric fate of C_3-C_6 hydroxyalkyl nitrates, *J. Phys. Chem. A*, *107*, 7809–7817.

Treves, K., L. Shragina, and Y. Rudich (2000), Henry's law constants of some β, γ and δ hydroxy alkyl nitrates of atmospheric interest, *Environ. Sci. Technol.*, *34*, 1197–1203.

Tyndall, G. S., R. A. Cox, C. Granier, R. Lesclaux, G. K. Moortgat, M. J. Pilling, A. R. Ravishankara, and T. J. Wallington (2001), The atmospheric chemistry of small organic peroxy radicals, *J. Geophys. Res.*, *106*, 12,157–12,182.

von Kuhlmann, R., M. G. Lawrence, P. J. Crutzen, and P. J. Rasch (2003a), A model for studies of tropospheric ozone and non-methane hydrocarbons: Model description and ozone results, *J. Geophys. Res.*, *108*(D9), 4294, doi:10.1029/2002JD002893.

von Kuhlmann, R., M. G. Lawrence, P. J. Crutzen, and P. J. Rasch (2003b), A model for studies of tropospheric ozone and non-methane hydrocarbons: Model evaluation of ozone related species, *J. Geophys. Res.*, *108*(D23), 4729, doi:10.1029/2002JD003348.

von Kuhlmann, R., M. G. Lawrence, U. Pöschl, and P. J. Crutzen (2004), Sensitivities in global scale modeling of isoprene, *Atmos. Chem. Phys.*, *4*, 1–17.

Wang, Y., D. J. Jacob, and J. A. Logan (1998a), Global simulation of tropospheric O_3-NO_x-hydrocarbon chemistry: 1. Model formulation, *J. Geophys. Res.*, *103*, 10,713–10,725.

Wang, Y., D. J. Jacob, and J. A. Logan (1998b), Global simulation of tropospheric O_3-NO_x-hydrocarbon chemistry: 3. Origin of tropospheric ozone and effects of non-methane hydrocarbons, *J. Geophys. Res.*, *103*, 10,757–10,767.

Wesely, M. L., D. R. Book, R. L. Hart, and R. E. Speer (1985), Measurements and parameterization of particulate sulfur dry deposition over grass, *J. Geophys. Res.*, *90*, 2131–2143.

Wild, O., and M. Prather (2000), Excitation of the primary tropospheric chemical mode in a global three-dimensional model, *J. Geophys. Res.*, *105*, 24,647–24,660.

Wild, O., X. Zhu, and M. J. Prather (2000), Fast-J: Accurate simulation of in- and below-cloud photolysis in tropospheric chemical models, *J. Atmos. Chem.*, *37*, 245–282.

Williams, J., V. Gros, B. Bonsang, and V. Kazan (2001), HO cycle in 1997 and 1998 over the southern Indian Ocean derived from CO, radon, and hydrocarbon measurements made at Amsterdam Island, *J. Geophys. Res.*, *106*, 12,719–12,726.

Yevich, R., and J. A. Logan (2003), Assessment of biofuel use and burning of agricultural waste in the developing world, *Global Biogeochem. Cycles*, *17*(4), 1095, doi:10.1029/2002GB001952.

Zhou, X., and K. Mopper (1990), Apparent partition coefficients of 15 carbonyl compounds between air and seawater and between air and freshwater; Implications for air-sea exchange, *Environ. Sci. Technol.*, *24*, 1864–1869.

A. Ito, Frontier Research Center for Global Change, JAMSTEC, Frontier Research Building 2F, 3173-25 Showa-machi, Kanazawa-ku, Yokohama-city, Kanagawa, 236-0001, Japan.

J. E. Penner and S. Sillman, Department of Atmospheric, Oceanic and Space Sciences, University of Michigan, Ann Arbor, MI 48109-2143, USA.